prosthesis

MDPI

Review

A Comprehensive Review of the Multifaceted Characterisation Approaches of Dental Ceramics

Hanan Al-Johani [1,2,*], Julfikar Haider [2,3,*], Julian Satterthwaite [2], Marcia Borba [2] and Nick Silikas [2]

[1] Department of Restorative Dentistry, Division of Biomaterials, Faculty of Dentistry, King Abdulaziz University, Jeddah 21589, Saudi Arabia
[2] Division of Dentistry, School of Medical Sciences, University of Manchester, Manchester M13 9PL, UK; julian.satterthwaite@manchester.ac.uk (J.S.); marcia.borba@manchester.ac.uk (M.B.); nikolaos.silikas@manchester.ac.uk (N.S.)
[3] Department of Engineering, Manchester Metropolitan University, Manchester M1 5GD, UK
* Correspondence: hamaljuhani1@kau.edu.sa (H.A.-J.); j.haider@mmu.ac.uk (J.H.)

Abstract: Ceramic dental restorative materials have growing popularity, albeit their brittle and stochastic nature are acknowledged shortcomings that impact the prosthesis lifespan. The mechanical performance of ceramics is dominated by the constitutional microstructural and fracture toughness mechanisms, as well as externally applied triggers. Thus, there is ongoing expanding research in the sphere of ceramic material engineering and thermal refinement, addressing concerns regarding toughness, machinability, reliability, stainability, and biodegradation. While the current trend in dental ceramic manufacturing has transitioned from micrometric crystalline sizes to submicrometric and nanometric ranges, there is an unclear understanding of the microstructural implications on ceramic behaviour. Therefore, this review covers the comprehensive characterisation approaches commonly employed in the scientific literature to describe the multifaceted performance aspects as well as clinical-related prerequisites of dental ceramics. Moreover, updated standardised testing parameters and performance thresholds pertaining to ceramic mannerisms are described in an attempt to translate their clinical applicability.

Keywords: dental glass ceramics; characterisation; flexural strength; fracture toughness; hardness; machinability; edge chipping; tribology; roughness; wettability; colorimetry; translucency; irradiance; microstructure; thermal analysis

Citation: Al-Johani, H.; Haider, J.; Satterthwaite, J.; Borba, M.; Silikas, N. A Comprehensive Review of the Multifaceted Characterisation Approaches of Dental Ceramics. *Prosthesis* **2024**, *6*, 1055–1090. https://doi.org/10.3390/prosthesis6050077

Academic Editors: Roberto Sorrentino, Fernando Zarone, Gennaro Ruggiero and Marco Cicciu

Received: 8 July 2024
Revised: 30 August 2024
Accepted: 2 September 2024
Published: 4 September 2024

1. Introduction and Review Methodology

Dental ceramics underwent significant developments in their composition, microstructure, and manufacturing processes, notably among the most recent polymer-infiltrated hybrid ceramics as well as lithium-based silicate glass ceramics and zirconia polycrystalline ceramics [1]. The superior biocompatibility, natural aesthetic appearance, improved mechanical performance, and established longevity have all played a role in the gaining popularity of dental ceramics, which extended the range of clinical applications. In vitro assessments are regarded as the foundation within the hierarchy of material appraisal, owing to their meticulous controllability and standardisation of testing variables. This review article provides an essential insight into the multifaceted material characterisation realm pertaining to dental ceramics, with a detailed focus on the mechanical, tribological, topographical, spectrophotometric, microstructural, and thermal criteria, taking into account the most recently introduced standards of the International Organisation for Standardisation (ISO 18675:2022), in addition to the updated ISO standards (ISO 6872:2023 and ISO 9693:2019) for dental ceramic materials [2–4]. The required thresholds for specific dental ceramic material-related properties have been highlighted for general dental practitioners to enhance their future evidence-based clinical judgements, thus improving overall patient quality of life.

The review methodology herein comprised of employing a search strategy (Table 1), beginning with defining inclusion and exclusion criteria, followed by screening appropriate abstracts, retrieving full text of studies from selected abstracts, and finally extracting the main outcomes/findings. Inclusion selection criteria involved articles written in English language and related to dental ceramics, including in vitro studies (comparative or experimental), technique reports, and review articles, whereas the exclusion criteria included any articles that failed to pass items described in the inclusion criteria. Electronic searches included literature evidence published up to June 2024.

Table 1. Search strategy for narrative review.

Database	Search Terms
PubMed/Medline	"Dental ceramics" OR "dental materials" OR "dentistry" OR "CAD/CAM" OR "Machinable dental ceramics" OR "Pressable dental ceramics" OR "Heat pressed dental ceramics" OR "Glass-ceramics" OR "Polycrystalline ceramics" OR "Hybrid ceramics" OR "Mechanical properties" OR "Flexural strength" OR "Fracture toughness" OR "Reliability" OR "Machinability index" OR "Brittleness index" OR "R-curve behaviour" OR "Edge chipping" OR "Hardness" OR "Friction" OR "Tribology" OR "Wear resistance" OR "Abrasion resistance" OR "Chemical solubility" OR "Topography" OR "Roughness" OR "Wettability" OR "Optical properties" OR "Spectrophotometry" OR "Colour" OR "Stainability" OR "Translucency" OR "Fluorescence" OR "Opacity" OR "Opalescence" OR "Whiteness" OR "Gloss" OR " Irradiance" OR "Spectroscopy" OR "Microscopy" OR "Crystallography" or "Fractography" OR "X-ray diffraction" OR "Differential scanning calorimetry" OR "Thermogravimetric analysis" OR "Thermal dilatometry"
Scopus	
Google Scholar	

2. Mechanical Characterisation

Appropriate in vitro simulation of the multi-directional masticatory forces significantly aids in the prediction of short-term clinical performance and long-term survival of ceramic restorations. Considering the brittle nature of dental ceramics and the absence of plastic deformation processes within, intraoral occlusal stresses can lead to repercussions ranging from subcritical crack growth to catastrophic failure. An assessment of resistance to bending, crack propagation, and indentation of ceramic materials can enhance the understanding of their mechanical behaviour and fracture mechanics.

2.1. Flexural Strength

The flexural strength of a ceramic material determines its resistance to bending forces, which are a combination of tensile, compression, and shear [5,6]. Considering dental ceramics are weaker under tension than under compression, flexural strength is a significant parameter to investigate. It can be measured by uniaxial tests, such as three-point bending or four-point bending, or biaxial tests, such as ball-on-ring, ring-on-ring, piston-on-ring, piston-on-three-balls, and ball-on-three-balls assemblies. These tests are all similar in that they are based on generating tensile stresses at the specimen surface opposite to where the compressive load is being applied. Then, a pre-existing critical flaw located in the area of maximum tensile stresses would propagate, leading to catastrophic failure. The three-point bending test has been traditionally advocated as the standard flexural strength test for dental ceramics because of its straightforward test design. Studies have reported higher flexural strength values obtained from three-point bending tests, in comparison to four-point bending tests, due to larger flaw-containing areas in the latter. Nonetheless, the main drawback of uniaxial flexural strength tests is the presence of flaws along the surface edges of the rectangular-shaped specimens [6]. Therefore, biaxial flexural tests have become increasingly utilised due to their central loading force, which disregards the effect of flaws on the edge surfaces [7]. Figure 1 illustrates the different flexural strength testing apparatuses.

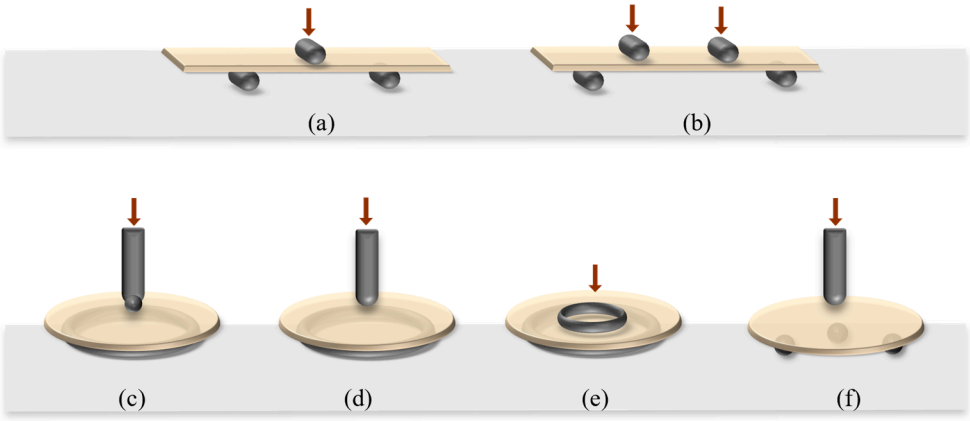

Figure 1. Flexural strength testing apparatus: (**a**) 3-point bending uniaxial flexural test, (**b**) 4-point bending uniaxial flexural test, (**c**) ball-on-ring biaxial flexural strength test, (**d**) piston-on-ring biaxial flexural strength test, (**e**) ring-on-ring biaxial flexural strength test, and (**f**) piston-on-three-balls biaxial flexural strength test. Tensile stresses are generated on the specimen surface opposite the compressive load (brown arrow(s)).

Commercial CAD/CAM ceramics are generally supplied in fixed geometries of either cuboidal blocks or disc-shaped blanks to accommodate for the rising trend of CAM/CAM machining in the dental market. The small dimensions of the CAD/CAM blocks (ranging from $8 \times 8 \times 15$ mm^3 in size I8 blocks up to $18 \times 16 \times 18$ mm^3 in size C16 blocks) might potentially fail to meet the size requirements of uniaxial flexural strength testing standards [8]. The ISO 6872 standard for ceramics tolerates span lengths at 12 mm (three-point bending) and 16 mm (four-point bending). However, bearing in mind the dependence of ceramic strength on volume (i.e., specimen size), these shorter span lengths could give rise to inherent testing errors that are significantly intensified by specimen miniaturisation [9]. In miniaturised uniaxial testing set-ups, extensive care is needed to ensure the precise positioning of the loading component as well as thorough edge chamfering of specimens, to prevent skewed distribution of the strength values [9]. On the other hand, the biaxial flexural test technique is not hindered by chipped-edge-induced stresses and exerts multiaxial stresses that better mimic intraoral forces. Noteworthy shortcomings of these rotationally symmetric biaxial testing methods are the prerequisite of an absolute flat parallel plane on the ceramic specimen surface and the inevitable presence of friction at the specimen and loading components interface [8]. The ball-on-three-balls (B3B) biaxial strength test configuration was developed to eliminate the friction component between the loading/supporting balls and the sandwiched ceramic specimen by the passive rolling of the loading balls upon specimen fracture [10]. B3B tolerates the testing of samples of rectangular geometries (plates), which offers a convenient solution to compute the strength of CAD/CAM ceramics delivered as blocks and is not altered by slight warping or flatness deviation $\leq 16\%$. The B3B testing apparatus provides a stress field with three-fold symmetry (in discs) or mirror symmetry (in plates) on the tensile surface of the ceramic specimen, after which the tensile load is transmitted by a loading central ball within a fixed contact area, creating stresses as a function of the elastic moduli of both the loading ball and the tested specimen (Figure 2). If considerable specimen deformation occurs upon loading, this could change the contact area with the loading ball and, in turn, skew the stress distribution. Materials with lower elastic moduli, such as dental composites, exhibit greater deformations and a larger contact area than materials with higher elastic moduli, such as ceramics; hence, greater precautions must be taken when testing the former [8,11].

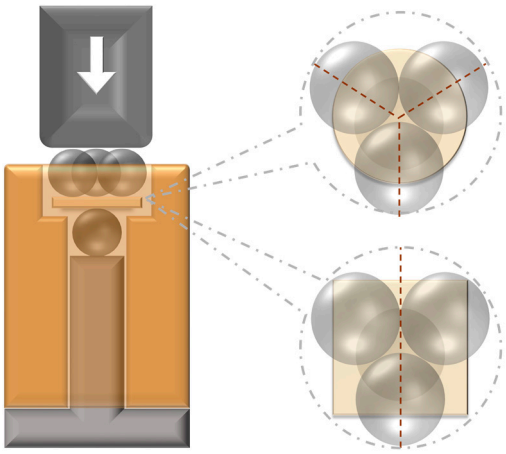

Figure 2. B3B testing apparatus demonstrating three-fold symmetry in disc-shaped specimens (**upper**) and mirror symmetry in rectangular plates (**lower**). Tensile stresses are generated on the specimen surface opposite to the compressive load (white arrow).

The calculation of flexural strength relies on finite element analysis to obtain the function δ, which is factored by independent variables: the dimensional ratio related to the support radius (R_a), the supporting ball radius (R_b), the radius of the specimen R (R_a/R), the thickness-to-specimen radius ratio (t/R), and the tested material Poisson's ratio (v). Due to excess material on plate specimen corners, this causes a stiffening effect within the specimens, hence altering the value of function δ via finite element analysis. Therefore, in specific plate dimensions of 12 × 12 mm^2 in thickness t, the function δ is measured as follows [8]:

$$\delta = 0.323308 + \frac{\left[[(1.30843 + 1.44301v)]\left[1.78428 - 3.15347\left(\frac{t}{R_a}\right) + 6.67919\left(\frac{t}{R_a}\right)^2 - 4.62603\left(\frac{t}{R_a}\right)^3\right]\right]}{\left[1 + 1.71955\left(\frac{t}{R_a}\right)\right]} \quad (1)$$

$$R_a = \frac{2\sqrt{3R_b}}{3} \quad (2)$$

Subsequently, the flexural strength (σ) in B3B is reported as the maximum stress created on the tensile side of the specimen at fracture, calculated by the following equation:

$$\sigma = \delta\, F_{max}/t^2 \quad (3)$$

Measurement errors of the B3B testing method are ≤2% and mainly stem from miscalculations of specimen dimensions as well as the intrinsic uncertainty of the function δ computed by the linear elastic model. Further measurement errors are <1% and are prompted by misorientation of loading balls, improper force measurement, inaccurate specimen geometry, and incorrectly positioning the rectangular plate specimens in relation to the loading balls. However, since these factors minimally influence the final strength values (i.e., ≤2%), their errors in measurements can be neglected. On the other hand, major error contributors (>2%) are the specimen thickness and Poisson's ratio. Thicker specimens of low elastic modulus will require higher fracture loads due to the larger contact area, while thinner specimens will experience greater deflection; hence, customised finite element analysis will be needed in these specific circumstances [12].

2.2. Reliability

Due to the brittle nature of dental ceramics, their ability to resist fracture under stress is highly influenced by the size and distribution of an intrinsic flaw population. Considering that larger sized flaws are more likely to cause failure yet are not normally distributed

within the Gaussian curve, strength measurements of ceramics are statistically analysed via Weibull statistics rather than statistics based on a Gaussian distribution. The following equation is used for Weibull fracture strength analysis:

$$P_f(\sigma) = 1 - \exp\left[-\left(\frac{\sigma}{\sigma_0}\right)^m\right] \quad (4)$$

where P_f (σ) is the probability of failure for a given flexural strength, σ is the fracture strength, σ_0 is the characteristic strength at the 63.2% fracture probability, and m is the distribution shape parameter, known as the Weibull modulus: m is characterised by the slope of the curves in Weibull plots, which imply the reliability of a given material. A higher m is associated with a steeper curve and a narrow distribution of flaws, indicating higher reliability of the material [13]. Upper and lower limits of the 95% confidence intervals for σ_0 and m can be calculated following the EN 843–5:2007 [14]. In general, large sample sizes are required for ceramic material strength assessment to foster adequate confidence limits of minimal bias risk [15]. To correct for statistical bias errors, an unbiased estimate of the Weibull modulus was obtained by correction of the biased Weibull modulus by means of an appropriate unbiasing function using the following equation:

$$\hat{m}U = \hat{m} \times UF \quad (5)$$

where $\hat{m}U$ represents the unbiased Weibull modulus, $\hat{m}$ is the biased Weibull modulus, and UF is the unbiasing f actor as a function of the sample size obtained from BS EN ISO 20501:2022 [16]. In accordance with the Weibull probability theory of ceramic flaw distribution, larger sized specimens will have a greater likelihood of enclosing larger inherent flaws, thereby resulting in lower flexural strength outcomes. Based on this assumption, direct comparisons between strength values of different testing apparatuses or dissimilar specimen dimensions violates the principles of Weibull probability and thus should be avoided [8]. Nonetheless, in order for dental clinicians to correctly interpret the strength data obtained from two different in vitro testing methods (test a and test b), the strength values can be scaled [17]. When specimens' fractures are caused by volume flaws then the scaling of strength values is performed as a function of the effective volume (V_{eff}):

$$\sigma_a = \sigma_b \left[\left(\frac{V_{effb}}{V_{effa}}\right)^{1/m}\right] \quad (6)$$

where σ_a is the flexural strength obtained in test a, σ_b is the flexural strength obtained in test b, V_{effa} is the effective volume in test a, V_{effb} is the effective volume in test b, and m is the Weibull modulus. On the other hand, if surface flaws are the cause of fracture, then the scaling of strength data can be performed via the effective surface (S_{eff}):

$$\sigma_a = \sigma_b \left[\left(\frac{S_{effb}}{S_{effa}}\right)^{1/m}\right] \quad (7)$$

where S_{effa} and S_{effb} are the effective surfaces in test a and test b, respectively. The effective volume and effective surface parameters are related to the specimen geometry (height, length, and width) and differ according to the type of flexural test employed (e.g., three-point bending, four-point bending, or B3B) [18].

2.3. Fracture Toughness

Fracture toughness (K_{Ic}) describes the ability of brittle materials, i.e., dental ceramics, to withstand unstable crack propagation from a pre-existing flaw when the material is loaded under tension [19]. Griffith introduced K_{Ic} by identifying that stress in a loaded brittle material is concentrated at the tip of a flaw and is proportional to the length of this

flaw. Irwin expanded this theory to ductile materials, identified the stress intensity factor "*K*", and concluded that brittle fracture takes places when the stress intensity at a crack of length "a_c" exceeds the critical stress intensity factor, i.e., $K > K_{Ic}$. Therefore, K_c symbolises the fracture toughness, and the subscripts I, II, or III denote mode fracture that occurs. The different fracture modes include mode I (crack opening by tensile forces perpendicular to the crack direction), mode II (shear/sliding force), and mode III (tearing/torsional force; Figure 3) [20,21].

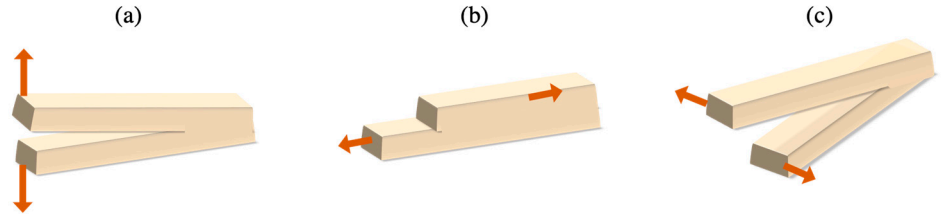

Figure 3. Different failure modes. (**a**) mode I (tensile force), (**b**) mode II (shear force), and (**c**) mode III (torsional force). Orange arrows signify the direction of applied load.

K_{Ic} can be measured by fracture testing methods with predetermined cracks introduced on the surface of specimens (e.g., single-edge v-notched beams, surface-crack-in-flexure method, double cantilever beam, compact tension, single-edge pre-cracked beam, chevron notch short rod, and the notchless triangular prism test) [22,23] or by indentation-based approaches (e.g., Vickers or Knoop indentation fracture tests; Figure 4) [24,25]. A main shortcoming of indentation fracture tests is the scattered K_{Ic} values that are obtained due to the residual stresses surrounding the crack propagation. Hence, indentation-based methods can provide a comparison between materials but cannot identify the exact fracture toughness value of a specific material, as the K_{Ic} values measured with the indentation-based techniques result in 48% variations from their true K_{Ic} values [15,26].

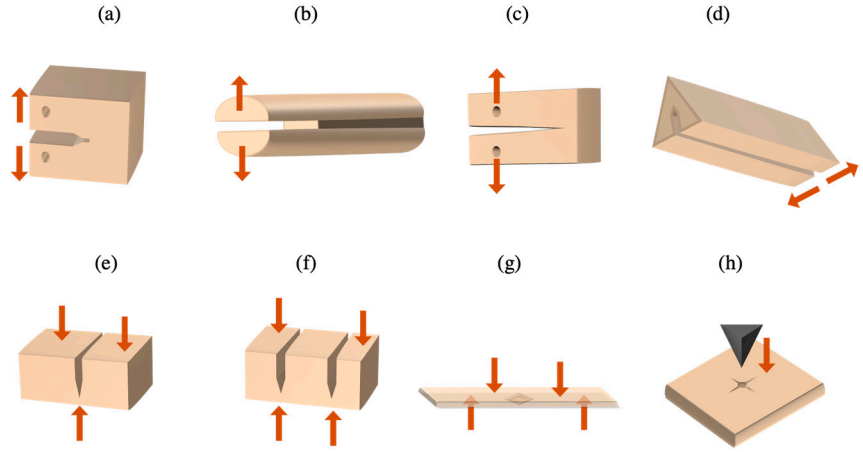

Figure 4. Different fracture toughness apparatuses: (**a**) compact tension, (**b**) chevron notch short rod, (**c**) double cantilever beam, (**d**) notchless triangular prism, (**e**) single-edge v-notched beam, (**f**) single-edge double-notched beam, (**g**) surface-crack-in-flexure, and (**h**) indentation-based fracture toughness method. Orange arrows represent the direction of fracture load.

Recently, fracture toughness of dental ceramics has been measured by the ball-on-three-balls test (*B3B-*K_{Ic}), akin to the surface-crack-in-flexure methodology. *B3B-*K_{Ic} can be executed on rectangular plates as well as disc-shaped specimens and has reported comparable results to standard K_{Ic} measuring techniques [27–29]. Using a Knoop indenter tip, a semi-elliptical crack is created on the surface of a specimen opposite the compressive

loading stresses, with depth a and full-width $2c$ pre-crack dimensions (Figure 5), and $B3B\text{-}K_{Ic}$ (MPa$\sqrt{\text{m}}$) is calculated with the following equation:

$$B3B\ K_{Ic} = \sigma \times Y_{B3B} \times \sqrt{\pi a} \quad (8)$$

where σ is the B3B flexural strength of specimen, with thickness t, Poisson's ratio v, crack depth a, and half-crack length c, R_a is the support radius, and Y_{B3B} is the geometric factor specific for $B3B\text{-}K_{Ic}$, as calculated via finite element analysis [30] based on the specimen geometry:

$$Y_{B3B} = \left(v, \frac{a}{c}, \frac{a}{t}, \frac{t}{R_a}\right) \quad (9)$$

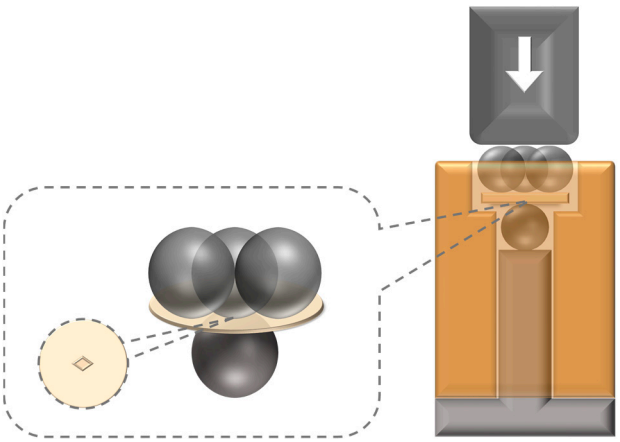

Figure 5. Schematic depiction of the ball-on-three-balls test fracture toughness testing apparatus with the pre-cracked specimen surface in tension.

According to the BS EN ISO 6872:2023 standard [3], the clinical indications of dental ceramics are ultimately governed by their mechanical performance (Table 2), specifically, their flexural strength (σ) and fracture toughness values (K_{Ic}).

Table 2. Dental ceramic mechanical thresholds and corresponding clinical applications.

Flexural Strength (σ) MPa	Fracture Toughness (K_{Ic}) MPa.m$^{1/2}$	Clinical Indication
50	0.7	1. Adhesively cemented monolithic single-unit anterior prosthesis. 2. Veneering of metal or ceramic substructures.
100	1.0	1. Adhesively cemented monolithic single-unit anterior or posterior prosthesis. 2. Adhesively cemented partially or fully covered substructure for single-unit anterior and posterior prosthesis.
300	2.0	1. Adhesively or non-adhesively cemented monolithic single-unit anterior or posterior prosthesis, and for three-unit prostheses not involving the molar region. 2. Adhesively or non-adhesively cemented partially or fully covered substructure for single-unit anterior or posterior prosthesis, and for three-unit prostheses not involving molar.

Table 2. *Cont.*

Flexural Strength (σ) MPa	Fracture Toughness (K_{Ic}) MPa.m$^{1/2}$	Clinical Indication
500	3.5	1. Monolithic three-unit prostheses involving molar restoration. 2. Partially or fully covered substructure for three-unit prostheses involving molar restoration.
800	5.0	1. Monolithic partially or fully covered substructures for four or more units. 2. Fully covered substructure for prostheses involving four or more units.

2.4. R-Curve Behaviour

Subcritical crack propagation within dental ceramics is a time-dependent phenomenon wherein long-term repetitive loading fosters strength degradation. Dental ceramics' toughening mechanisms, such as crack shielding, crack bridging, crack branching, and phase transformation, are able to enhance the fracture toughness (i.e., crack resistance) as the crack dimension increases. This distinct mannerism is termed crack growth resistance curve behaviour i.e., R-curve behaviour. Ceramics exhibiting R-curve behaviour are deemed more reliable (less scatter in strength values) and of predictable longevity. R-curve behaviour can be inferred from the surface-crack-in-flexure strength testing method, wherein ceramic specimens are indented with different loads then flexural-strength-tested (e.g., four-point bending and B3B). Upon plotting the flexural stress against the indentation load in a double-logarithmic scheme, with a least-square linear regression curve fitted through the data points, R-curve behaviour can be assumed if the slope of this fit line differs significantly from $-1/2$. Thereafter, fracture toughness (MPa·m$^{1/2}$) is computed and plotted against the increasing crack sizes to construct R-curve behaviour plots pertaining to individual ceramic materials. Information obtained from the R-curve shape, steepness, and crack extension range can provide valuable insight regarding ceramic microstructure and fracture mechanics [1,31,32].

2.5. Machinability

In compliance with the trend for subtractive manufacturing of computer-aided design/computer-aided manufacturing (CAD/CAM), most dental ceramics available in the market are presented in the form of machinable blocks of fixed geometry and with precise crystallisation and sinterisation guidelines. The recently introduced ISO standards (ISO 18675:2022) were proposed to evaluate the machining tolerances and post-machining distortion in CAD/CAM ceramics [2]. Polycrystalline zirconia and alumina machinable blocks can be supplied as powder-pressed (i.e., green blanks) or partially sintered, which inevitably results in 20–35% volumetric shrinkage upon complete sintering into a fully dense blank. A parameter commonly reported by manufacturers of machinable ceramics is the shrinkage factor (d), a measure of the three-dimensional changes in volume coinciding with sintering, such as green or partially sintered blanks. Prior to sintering, the width, thickness, and length of the specimens are recorded as w_1, b_1, and l_1, respectively, and after sintering is completed, the dimensions are remeasured (w_2, b_2, and l_2) and, subsequently, d is computed, as follows:

$$d = (d_w + d_b + d_l)/3 \quad (10)$$

where $d_w = w_1/w_2$, $d_b = b_1/b_2$, and $d_1 = l_1/l_2$.

The shrinkage factor facilitates the calculation of the percentage of overestimation needed to obtain dental ceramic restorations of an accurate fit. Another important consideration when sintering is the possibility of warpage that occurs in green or partially sintered blanks. Warpage (e) is the degree to which a blank acquires a uniformly flat surface

after final sintering or post-machining processing (Figure 6). The percentage of warpage of ceramics can be recorded by calibrated digital micrometres, as follows:

$$e = \left(\frac{c}{x}\right) \times 100 \quad (11)$$

where c denotes the clearance between a flat surface and maximum point of warpage and x denotes the distance between two ends of the ceramic bar [2].

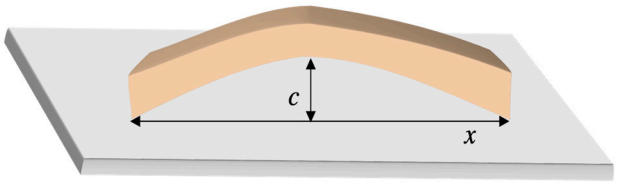

Figure 6. Schematic representation of warpage in a fully sintered dental ceramic bar.

The machinability index (i.e., machining difficulty) and brittleness index (i.e., susceptibility to brittle fracture) have been frequently employed in the literature when describing machinable ceramic materials [33,34]. A quantification of the intact minimal machined thickness of a dental ceramic can be determined through the merlon fracture test, wherein fractured merlons (i.e., free-standing walls) signify that the milling process is detrimental to dental restorations of similar margin thicknesses [2]. The test specimen geometry consists of a round hollow ring with a solid bottom (analogous to the occlusal surface of a crown) and four protruding merlons (analogous to crown margins; Figure 7). Data for the merlon fracture test specimen geometry are provided by the American Dental Association as STL files to be imported into the equipped CAD/CAM software, with a selection of merlon wall thicknesses ranging from 0.1 to 0.5 mm. Subsequently, specimens are machined with the milling bur direction parallel to that of the merlon walls. After milling, intact merlons and specimen bottoms are counted in addition to fractured merlons (if >1/3 of the merlon tip is lost) and fractured specimen bottoms (have a hole visible to the naked eye) [2,35].

The machinability of dental ceramics can also be reported as a function of their brittleness index (*BI*), which is the ratio between their hardness (GPa) and the critical strain energy release rate (J/m^2):

$$BI = H/G_{IC} \quad (12)$$

and

$$G_{IC} = K_{Ic}/E \quad (13)$$

where H denotes the hardness, G_{IC} is the critical strain energy release rate, K_{Ic} is the fracture toughness, and E is the elastic modulus.

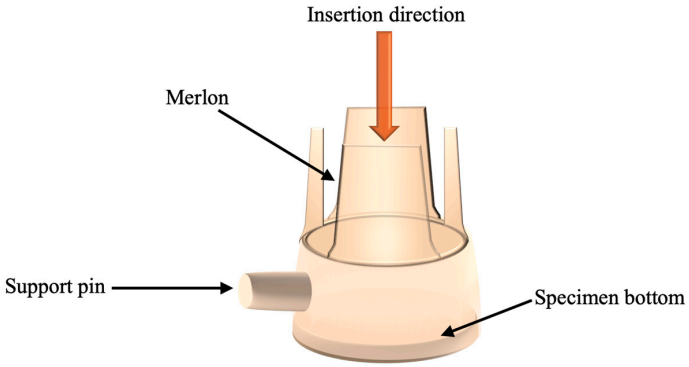

Figure 7. Specimen geometry in the merlon fracture test apparatus.

A lower *BI* indicates the capacity for plastic deformation, whereas a higher *BI* implies brittle fracture behaviour. In general, adequate machinability of dental ceramics can be fostered when $BI < 4.3\ \mu m^{-1}$ and can be enhanced by ultrasonic vibrations [36–39].

2.6. Edge Chipping

Chipping of dental ceramic restorations occurs as a result of the proximity of intraoral forces to the restoration edge, leading to the detachment of ceramic flakes. Edge chipping resistance (R_{eA}) can be directly measured with a customised device (e.g., CK 10, Engineering Systems, Nottingham, UK) utilised for the crack detection of brittle materials, such as dental ceramics, wherein an indenter chips away the ceramic at progressively increasing distances in relation to an interface edge of the material bulk (Figure 8). Universal testing machines have also been employed for edge chipping tests, in which an indenter of a predetermined load is applied at a specific distance away from the edge, and the force required to generate a chip is subsequently recorded. Other edge chipping parameters include the chipping factor (CF%), edge chipping toughness (T_e), edge chipping strength (S_E), and the applied force versus edge distance (F vs. d). In general, the forces leading to ceramic chipping depend on the geometry and direction of the loading component as well as the hardness and fracture toughness of the restoration [40,41].

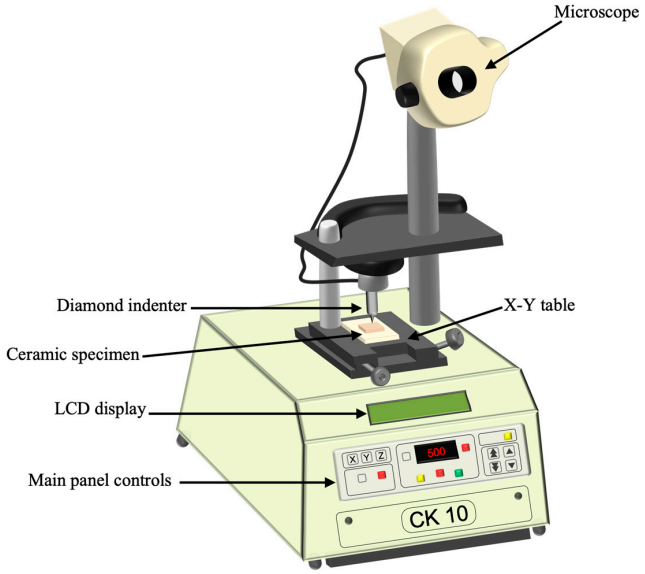

Figure 8. Schematic representation of the edge chipping testing device.

2.7. Hardness

Hardness of dental ceramics is the resistance of the surface to indentation or scratching and is calculated as the maximum applied force per unit area of indentation. Hardness can be used as an indicator of various properties, including wear resistance and polishability. It can be measured by multiple surface hardness tests that differ in their indenter shape and loading force applied. Macro-indentation tests apply forces between 2 and 30 kN, micro-indentation tests apply forces less than 2 N with indentation depth $\geq$ 0.2 mm, while nano-indentation tests generate indentations < 0.2 mm in depth. Micro-indentation tests are more commonly used to test the hardness of dental materials. Popular ceramic hardness testing methods are the Vickers, Knoop, and Martens hardness tests [5,42–44]. Vickers and Knoop hardness tests are dependent on the load and dwell times; hence, difficulties may be encountered when recording measurements since upon removal of the indenter, the measurement of the resultant indentation is limited by the reduced resolution of the optical system, the indentation perception of the operators, and the elastic recovery of the material [45,46].

The Vickers hardness test is comprised of a square-based pyramid diamond indenter with opposite sides meeting at the apex at 136°. Hardness is calculated from the surface area of a square-shaped indentation that is produced when the indenter is forced into the tested surface for a specific dwell time. The resultant indentation in the Vickers hardness test has the same geometry for different tested materials and testing loads and can be

used to measure microhardness for a wide range of materials, such as cast alloys, brittle materials, and tooth structure. On the other hand, the Knoop hardness test consists of an indenter that is a rhombic-based pyramidal diamond with diagonals that are seven times longer than its width, generating an elongated indentation. The Knoop hardness test can measure a broad range of hardness values by applying different loading forces, and thus can be used in brittle material of minimal thickness [42,44,47].

The Martens hardness test (Figure 9), formerly known as the Universal hardness test, is appropriate for hardness testing of the majority of solid materials, as it takes into consideration the elastic and plastic deformation of materials. This is due to the fact that the hardness value is achieved from the indentation depth beneath the working load and is not as affected by the specimen's viscoelastic or optical properties. Furthermore, the geometry of the indenter (identical to the Vickers pyramidal diamond indenter) provides a hardness value that is independent from the force chosen in testing [43]. Martens hardness tests can be performed by macro-, micro-, and nano-ranged measurements, and testing can be carried out by controlling the force or the indentation depth. During the test, the vertex of the diamond indenter is forced onto the specimen surface and then is held in place for a specific amount of time. The testing force, F, and indenter displacement, h, are measured directly throughout the testing while both increasing and decreasing the test force. The indenter displacement denotes the total elastic displacement in the surface as well as the plastic depth of the impression. In standard conditions, the test force is placed gradually, and the distance between the centre of each indentation and the edge of the specimen is maintained at a space $\geq 40\times$ greater than the indentation depth. Subsequently, both the applied force and indentation are simultaneously measured, as well as other parameters, including Martens hardness (HM, N/mm^2) and the indentation modulus (E_{IT}, kN/mm^2) [48–50]:

$$HM = \left[\frac{F}{A_s(h)}\right] \tag{14}$$

$$E_{IT} = \left(1 - v_s^2\right)\left[\left(\frac{1}{E_r}\right) - \left(\frac{1 - v_i^2}{E_i}\right)\right] \tag{15}$$

where F is the test force (N), $A_s(h)$ is the surface area of the indenter at distance h from the tip (mm^2), v_s and v_i are Poisson ratios of the specimen and indenter, respectively, while E_r and E_i are the moduli of the indentation contact and the indenter, respectively.

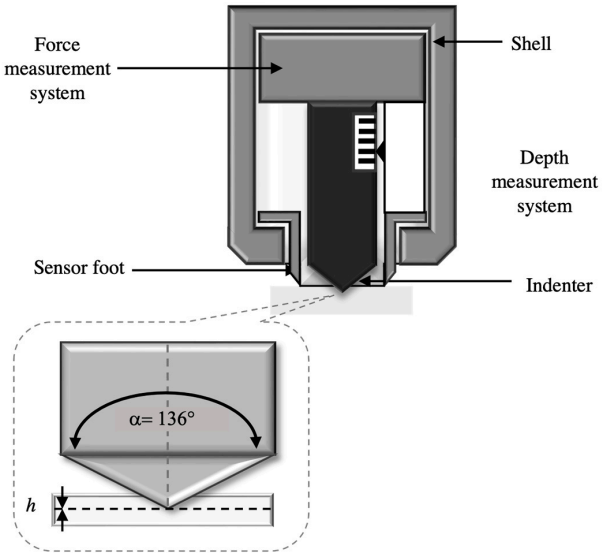

Figure 9. Schematic representation of Martens hardness testing apparatus (adapted from Shahdad et al. [46]).

2.8. Research Trends in Mechanical Characterisation of Dental Ceramics

Clinical relevance of the mechanical characterisation is derived from in vitro to in vivo extrapolations. Flexural strength tests are commonly employed in the literature due to their relatively straightforward specimen design and test apparatus [6,7]. Nonetheless, the quasi-static nature of these bending tests abstains from providing information regarding crack resistance and deformation during high-strain-rate loading. Fracture toughness data of dental ceramics has been reported to be a better predictor of their clinical longevity than flexural strength data, as the former can yield information related to unstable crack growth [51]. However, a noteworthy drawback of fracture toughness testing is the strenuous and time-consuming specimen preparation aspect. Machinability and brittleness indices yield significant information regarding the minimal thickness requirements of novel CAD/CAD dental ceramics indicated for veneers and in patients with limited occlusal clearance. Nevertheless, there are a variety of different indices used to quantify the brittleness in the literature [39], which could render difficulty in clinical inferences. Hardness tests can aid in interpreting the degree of wear resistance of dental ceramics, albeit not all hardness tests can be employed on dental ceramics due to their brittle character, such as the Rockwell and Brinell hardness tests [5,42], and hence they were not explored herein. Furthermore, relying on an objective approach, such as the Martens hardness test, is preferred to subjective methods (i.e., Vickers and Knoop) seeing as the latter could be negatively influenced by the microcracks observed along the diagonals of the indentation [50].

Bearing in mind that each mechanical characterisation approach serves a dedicated purpose, thus, they cannot be ranked in terms of favourable versus unfavourable approaches. Irrespective of the employed methodology, the implementation of artificial aging prior to the mechanical characterisation of dental ceramics can complement the clinical applicability of the presented testing methodologies herein.

3. Tribological Characterisation

Considering the dynamic nature of the oral environment, dental ceramic restorations are relentlessly exposed to thermal, mechanical, and chemical stresses, ranging from natural conditions (humidity, pH fluctuation, load cycles, temperature variation, and antagonistic contact) to prophylactic factors (toothbrush abrasion and mouthwash erosion) to pathologic elements (bruxism, gastroesophageal reflux disease, and excessive acidic beverage consumption). Thereby, dental ceramic material loss is exacerbated as a function of these patient-related environmental factors. ISO 14569 standards illustrate the variety of methodologies employed to investigate the wear caused by toothbrush abrasion (ISO/TR 14569-1:2007) and that caused by two- and/or three-body contact (ISO/TS 14569-2:2001) [52,53]. Direct tribological quantification of dental ceramics can be accomplished through tribometers with differing testing apparatuses that mimic two-body or three-body wear. Tribometers differ in terms of the loading component geometry as well as the direction of movement (sliding, or sliding plus impact), and thus can be classified as reciprocating tribometers (e.g., pin-on-disc, ball-on-3-flat, and sphere-on-plate), ball-crater tribometer, or chewing simulators (Figure 10) [54]. Repercussions of antagonistic wear can be assessed indirectly through qualitative analysis of surface topography of dental ceramics obtained from profilometer scanners, confocal laser microscopy, scanning electron microscopy, atomic force microscopy, quantitative light-induced fluorescence, or nanoindentation [55–57]. Among the tribological parameters reported in the literature are the coefficient of friction, specific wear rate, wear volume loss, and chemical solubility.

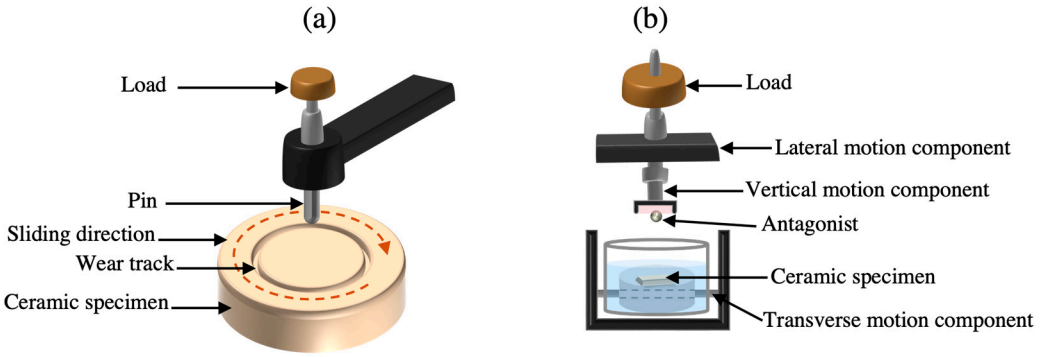

Figure 10. Schematic representation of tribometer apparatuses: (**a**) the pin-on-disc (sliding motion only) and (**b**) the chewing simulator (sliding and impact movements).

3.1. Coefficient of Friction

The coefficient of friction (COF) represents the ratio of the frictional force (F) withstanding motion between two contacting surfaces to the normal force (N) that presses the two contacting surfaces towards each other. The COF parameter of dental ceramics is usually automatically calculated by software equipped within the tribometer devices throughout the frictional episodes. In general, reduced wear potential of dental ceramics is found when their COF resembles that of the natural dentition [55].

3.2. Worn Volume and Specific Wear Rate

The degree of volumetric loss that occurs within a dental ceramic substrate due to wear mechanisms, i.e., worn volume, is an important indicator of its longevity. Worn volume (ΔV) can be quantified as follows:

$$\Delta V = \frac{\Delta m}{\rho} \tag{16}$$

where Δm is the change in mass (before and after the wear test) and ρ is the density of the ceramic [52]. Volume loss can also be quantified using specific software, in which the three-dimensional virtual models of the specimens before and after the test are overlapped and subtracted using methods such as confocal laser scanning microscopy [58].

The wear rate of dental ceramics depends on their microstructures, elastic modulus, fracture toughness, as well as the occlusal forces and opposing substrate material [59]. The specific wear rate (k) can be computed by the following equation:

$$k = \frac{\Delta V}{W \times S} \tag{17}$$

where ΔV is the worn volume (mm^3), W is the normal applied load (N), and S is the total sliding distance (m) [55].

3.3. Chemical Solubility

Exposure to acidic solutions, such as food simulating liquids, bleaching mouth rinses, or gastric juices, presents a risk for surface and bulk degradation of dental ceramics. The degree of erosion susceptibility differs based on the pH of the corrosive media, acidic challenge duration, as well as the material type, thickness, and anatomical location of the ceramic restoration [60]. Chemical solubility is a significant parameter that can aid in predicting the clinical survival of dental ceramics and can be quantified as follows:

$$CS = \frac{(m_1 - m_2)}{A} \tag{18}$$

where *CS* is the chemical solubility (μg/cm^2), m_1 and m_2 are the ceramic sample mass (μg) before and after exposure to an acidic challenge, respectively, and *A* is the specimen surface area (cm^2).

According to the ISO 6872:2023 standards, chemical solubility should not exceed 100 μg/cm^2 in the case of ceramics employed as veneering or monolithic restorations, whereas the chemical degradation of ceramic frameworks should not surpass the 2000 μg/cm^2 limit [3].

3.4. Research Trends in Tribological Characterisation of Dental Ceramics

Bearing in mind the vast amount of literature regarding artificial chewing simulation, an ideal reproduction of human masticatory movements has not yet been achieved to date considering that no simulator has incorporated both maxillary and mandibular complete arches; conversely, single antagonists of varying materials (enamel, stainless steel, tungsten carbide, steatite, and resin) have been employed [61]. Furthermore, a comprehensive model comprising the multifactorial fluctuating intraoral conditions (humidity, temperature, and pH) has not yet been delivered, thus contributing to the difficulty in standardisation of these thermodynamic testing methodologies. Hence, when comparing data from such studies, exact values should not be compared; instead, trends should be observed, and clinical judgements resolved accordingly. Nonetheless, tribological testing of dental ceramics is advantageous in its ability to incorporate underlying processes of lubrication, friction, and wear of occluding surfaces that interfere with ceramics' performance inside the oral environment [62].

Determining the degree of dental ceramics' chemical solubility as a function of exposure to various acidic agents is beneficial in understanding the risk of the erosive susceptibility of ceramic restorations in patients with high intraoral acidic challenges. A notable limitation of the ISO 6872:2023 chemical solubility approach is its sole dependency on the total surface area of tested specimens ($\geq$30 cm^2) without further indications regarding sample size or individual specimen dimension or geometry [3]. It has been reported that higher chemical solubility is detected in cubic-shaped specimens than in spherical geometric specimens, and reduced individual surface areas dissolve at greater rates than in larger sizes. Hence, this renders comparisons between chemical solubility data to be inaccurate. A recently proposed modification to the ISO 6872 reports that minimal physical handling during dental ceramic specimen transfer enhances the reproducibility of chemical solubility measurements [60].

4. Surface Topographical Characterisation

A smooth surface texture of a dental ceramic restoration is imperative to the clinical success: rougher surfaces increase the likelihood of interacting with the surrounding oral environment, impacting hydrophilic and light transmission capacities. Ceramic restorations with high surface roughness (>0.2 μm) have been associated with higher plaque accumulation, antagonistic wear of the natural dentition, and human tactile perceptibility [63–65].

4.1. Surface Roughness

Surface roughness signifies the height fluctuations of a surface area, depicted by peaks and valleys of a wavelength in relation to a parallel reference plane. There are multiple roughness parameters that can communicate the texture of a surface by measuring different height points within a defined surface area, in which the lower roughness values indicate a smoother surface texture. Cross-sectional roughness profiles yield two-dimensional parameters (e.g., R_a, R_q, and R_t), while topographic maps yield three-dimensional parameters (e.g., S_a and S; Figure 11). S_a is the average roughness value of the profile's departure from the mean reference line, within a specific sampling area. S_q is the square root of the mean of all height deviations, and S_q magnifies any odd height deviations in a specific surface; hence, this parameter is more accurate than S_a. Additional roughness parameters include S_z (average greatest peak-to-valley height of successive sampling areas) and S_p (maximum profile peak height above a mean line within the sampling area) [66].

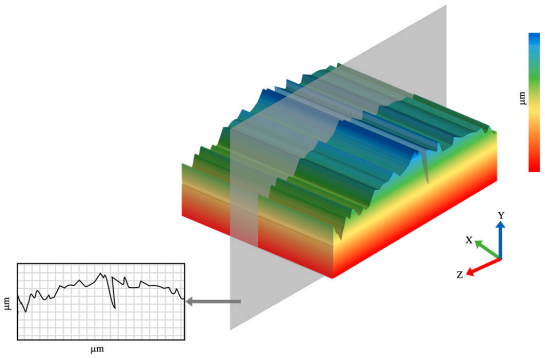

Figure 11. Schematic representation of 2D roughness profiles (**left**) and 3D topographic maps (**right**).

Surface roughness of dental ceramics can be analysed via contact or non-contact methods. Contact methods include the surface roughness tester, stylus profilometer, and atomic force microscopy (in static mode). The main drawback of these devices is the potential abrasion of the specimens by the profilometer stylus; hence, forces must be applied at levels below the hardness values of the specimens tested. Non-contact methods include the optical profilometer, confocal microscopy, scanning electron microscopy, laser reflectivity, and atomic force microscopy (in dynamic mode). The passivity in non-contact devices as well as the small diameter of the coupled laser scanner (<100 mm) provides surface topography measurements of higher accuracy [66–68]. The non-contact optical profilometer (Figure 12) is commonly used to measure height and volume differences in surface topographies. It comprises of a light source that transmits polychromatic light within a special lens that splits the light beam into a full spectral field according to the different refractive indices of the white light components. Surface analysis is accomplished by splitting the emitted beam within the profiler into two rays: one aimed at a standardised reference mirror and the second aimed away towards the specimen surface. Each wavelength is focused on a point that resides at an exact distance from the sensor, forming a band of monochromatic imaging points. The ability of the sensor to detect the distance is achieved by correlating the central wavelength of the reflected beam with the height of the focused point. Subsequently, an image of the surface topography is formed by a scanning raster, with profiling rates up to 1000 measurements per second at a resolution of up to 5 nm [69–71].

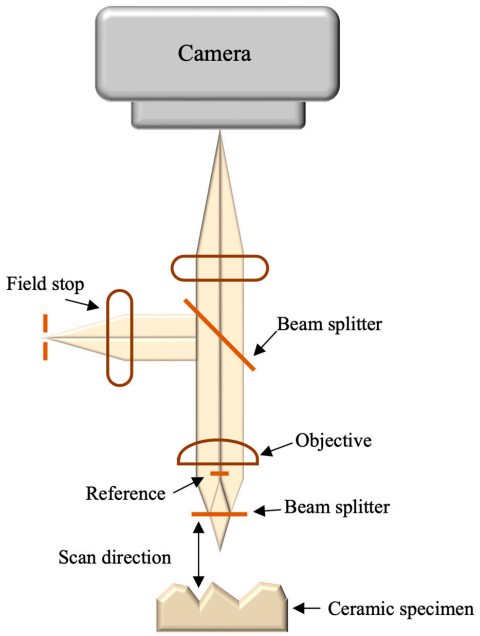

Figure 12. Schematic diagram of the non-contact optical profilometer (adapted from Baysan et al. [69]).

4.2. Wettability

Wettability is a measure of the ability of a liquid to sustain contact with a solid surface as a result of the balance between the adhesive (liquid-to-liquid) and cohesive (liquid-to-solid) intermolecular interactions (polar vs. nonpolar) [72]. Wettability of dental ceramics is reported in terms of the contact angle (θ°) of a liquid at the three-phase intersection of solid/liquid/vapor phases, computed by Young's contact angle equation based on the assumption of a topographically smooth substrate surface:

$$\cos\theta = \frac{(\gamma_{SV} - \gamma_{SL})}{\gamma_{LV}} \quad (19)$$

where γ is the interfacial tension, and subscripts S, V, and L represent solid, vapor, and liquid phases, respectively.

Upon calculating the contact angles, the degree of surface hydrophilicity is determined as super-hydrophilic ($\theta^\circ \approx 0^\circ$), hydrophilic ($0^\circ < \theta^\circ < 90^\circ$), hydrophobic ($\theta^\circ > 90^\circ$), or superhydrophobic ($\theta^\circ > 150^\circ$) [73]. Contact angle measurements are obtained via direct optical-based or indirect force-based techniques. Direct tests can be static, such as the sessile drop and captive bubble method, or dynamic, such as the tilting plate or needle method (with advanced, θ_A, and receding, θ_R, contact angles). Indirect methods include the Wilhelmy method and meniscus geometric shape analysis (Figure 13) [74–76]. The relationship between surface roughness and wettability can be explained by the Wenzel model (based on the assumption of complete liquid penetration into rough substrate surfaces) [77,78]:

$$\cos\theta^* = r\cos\theta \quad (20)$$

where θ^* is the measured contact angle of a rough substrate, r is the roughness coefficient (i.e., ratio of actual surface area to projected surface area), and θ is the contact angle of a smooth surface of the same substrate obtained from Young's contact angle equation (Equation (19)).

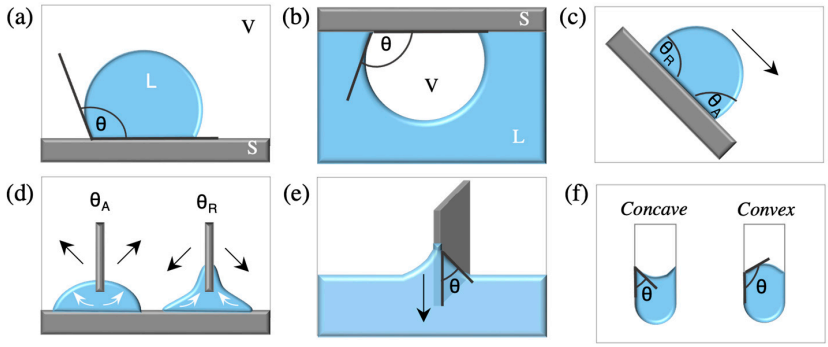

Figure 13. Methods of the contact angle measurements: (**a**) sessile drop, (**b**) captive bubble, (**c**) tilting plate, (**d**) needle method, (**e**) Wilhelmy method, and (**f**) meniscus shape method. Where S is the solid phase, L is the liquid phase, V is the vapor phase, θ is the contact angle, θ_A is the advancing contact angle, and θ_R is the receding contact angle.

According to the Wenzel model, in hydrophobic surfaces ($\theta^\circ > 90^\circ$), a smooth surface texture will enhance the wettability, whereas in hydrophilic surfaces ($\theta^\circ < 90^\circ$), rougher surface textures promote wettability.

Calculations generated from the measured contact angle (θ°) can quantify important parameters pertaining to the surface tension of a liquid and the surface energy of a solid. Within the field of adhesive ceramic bonding, a high surface energy on the substrate surface and low surface tension of the adhesive bonding agent are favoured for uniform spreading, while complete wetting is obtained when the surface tension of the adhesive is lower than that of the substrate surface [79]. Furthermore, the degree of hydrophilicity/hydrophobicity of ceramic substrates predicts the degree of bacterial adhesion, biofilm formation, and

staining susceptibility, i.e., hydrophobic surfaces exhibit lower surface energy and thus do not favour bacterial adhesion. On the other hand, the extent of wettability and surface energy of the intaglio ceramic surfaces can predict their bond strength and adhesion performance to the underlying substrate (Figure 14) [80].

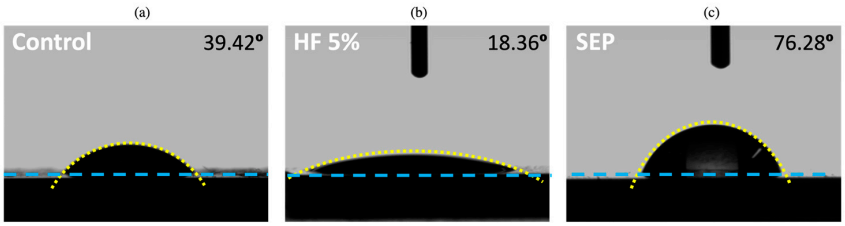

Figure 14. Representative contact angles (θ°) of saline drops deposited on the intaglio surface of a zirconia-reinforced lithium silicate glass ceramic (Celtra Duo, Dentsply Sirona): (**a**) without surface treatment, (**b**) after etching with 5% hydrofluoric acid, and (**c**) after etching with a self-etch primer. Blue dashed line denotes ceramic surface, and yellow dashed line denotes the saline droplet outline.

4.3. Research Trends in Topographical Characterisation of Dental Ceramics

Observing the topography of dental ceramics via optical methods is a non-destructive approach that yields important information regarding the impact of exposure ceramic restorations to surface treatments, coatings, and food simulating substances. Nonetheless, certain limitations hinder the accuracy in roughness and wettability data of dental ceramics, such as contaminated, uneven, or matte specimen surfaces.

Although it has been established that external surfaces of ceramic restorations should demonstrate hydrophobicity and low surface energy in order to reduce bacterial attraction and, in turn, biofilm accumulation [63–65], current evidence in the literature has proven to be insufficient in validating the correlation between the electrostatic condition, surface energy, and texture of dental ceramics with their bacterial adhesion susceptibly [80]. This presents an interesting opportunity for future research.

5. Spectrophotometric Characterisation

When visible-light wavelengths (350–800 nm) are emitted upon a dental ceramic, they can be transmitted, reflected, refracted, scattered, absorbed, or fluoresced (Figure 15). Light transmittance through glass matrix and crystalline phases is governed by their refractive indices ((RI) i.e., ratio of light velocity in a vacuum to its velocity in a medium). A greater RI match results in higher light transmission, whereas large RI mismatches hinder light passage. The degree of light transmittance is also regulated by the ceramic thickness and crystalline density: higher translucency is seen in thinner restorations of high glassy content, whereas thicker and polycrystalline ceramics display greater opacity. Furthermore, the surface texture impacts colour perception: smoother ceramic surfaces tend to reflect light, while rougher surfaces scatter light, resulting in a darker appearance than in the former [5,81,82].

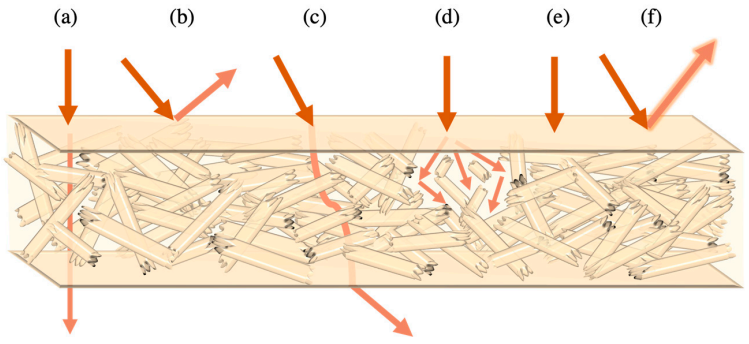

Figure 15. Possible pathways of visible light emitted on a lithium silicate-based ceramic: (**a**) transmission, (**b**) reflection, (**c**) refraction, (**d**) scattering, (**e**) absorption, and (**f**) fluorescence.

5.1. Colour Stability

Colorimetric quantification of dental ceramics has been traditionally performed by the three-dimensional Munsell colour system, comprised of three main attributes: value, V (vertical dark–light axis), hue, H (rotational pure-colour axis), and chroma, C (horizontal colour-saturation axis) [83]. The Commission Internationale de l'Eclairage introduced the CIE L*a*b* three-dimensional colour space, in which the coordinate L^* conveys the degree of lightness ($L^* = 100$) and darkness ($L^* = 0$), a^* denotes the amount of redness ($a^* > 0$) or greenness ($a^* < 0$), and b* represents the yellowness ($b^* > 0$) or blueness ($b^* < 0$; Figure 16). Ceramic colour alterations are seen upon aging or exposure to staining media and erosive environments; thus, the ability to maintain colour stability is an important factor in clinical longevity [84,85].

Colour stability of dental ceramics is commonly measured by computing the differences in each colour parameter (ΔL^*, Δa^*, and Δb^*) as a function of time (ΔE_{ab}) [85]:

$$\Delta E_{ab} = \sqrt{\Delta L^2 + \Delta a^2 + \Delta b^2} \quad (21)$$

Recently, the CIEDE2000 formula (ΔE_{00}) has been preferred to report the colour differences, as it conforms to the non-uniform nature of the CIE L*a*b* colour space by the incorporation of weighting functions for lightness (S_L), chroma (S_C), and hue (S_H), a rotation factor for hue and chroma interactions (R_T), and parametric factors that account for the illuminating conditions in lightness (K_L), chroma (K_C), and hue (K_H) [85,86]:

$$\Delta E_{00} = \sqrt{\left(\frac{\Delta L}{K_L S_L}\right)^2 + \left(\frac{\Delta C}{K_C S_C}\right)^2 + \left(\frac{\Delta H}{K_H S_H}\right)^2 + R_T\left(\frac{\Delta C}{K_C S_C}\right)\left(\frac{\Delta H}{K_H S_H}\right)} \quad (22)$$

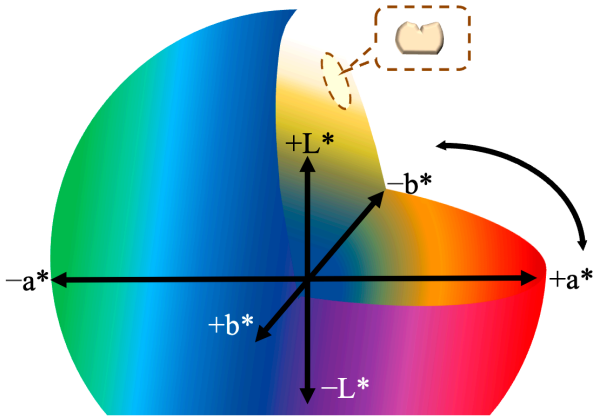

Figure 16. Depiction of dental ceramics within the CIE L*a*b* three-dimensional colour space, wherein L* represents lightness, a* and b* represent green–red spectrum and blue–yellow spectrum, respectively.

The smallest colorimetric difference (e.g., between two ceramic restorations) that is perceptible by the human eye is known as the perception threshold (PT), whereas a colour difference that is considered acceptable by the observer yet does not mandate the replacement of a restoration is known as the acceptability threshold (AT) [87]. Both thresholds, PT and AT, differ according to the colour difference formula employed (ΔE_{ab} versus ΔE_{00}) and according to the percentage (30%, 50%, and 90%) of clinicians agreeing with or refuting the perceptibility and acceptability values. For the ΔE_{ab} colour difference formula at 30%, 50%, and 90%, PT and AT are 1.0, 1.7, and 3.1, and 6.0, 3.7, and 1.8, respectively. Whereas for the ΔE_{00} formula at 30%, 50%, and 90%, PT and AT are 0.6, 1.1, and 2.2, and 4.8, 2.8, and 1.4, respectively. The most frequent PT and AT reported in the literature are at the 50% threshold, i.e., 50:50% PT is the value at which 50% of clinicians

detect a colour difference between two restorations, while the remaining 50% do not, and the 50:50% AT is the value at which 50% of clinicians indicate replacing the restoration for colour correction purposes, while the remaining 50% do not [87].

A variety of instruments can measure the colour and translucency of dental ceramics. The spectrophotometer is the most employed device, characterised by its ability to convert the light spectra components into colour coordinates based on the CIE colour system. It can measure the amount of reflected light energy from an object at 1–25 nm intervals along the visible-light spectrum and is composed of an optical radiation source, light disperser, optical measuring system, and software that converts transmitted/reflected light into analytical data signals that provide colour and translucency measurements for dental ceramics [88,89]. Double-beam spectrophotometers with integrated spheres are superior to their single-beam counterparts: the latter does not account for reflected light, and thus may yield inaccurate measurements in highly translucent ceramics due to the 'edge loss' phenomenon, wherein the incident light is scattered along the edges of ceramics instead of being reflected [90–92]. On the other hand, the integrated sphere in the former is a highly reflective barium-sulphate-coated chamber that uniformly scatters transmitted light and runs in a specular component included mode (for diffuse/specular reflectance measurements) or a specular component excluded mode (for diffuse reflectance measurements). Furthermore, the dual beams split incident monochromatic light into sample and reference beams, thereby simultaneously recording the total (collimated plus diffuse) transmitted light through the sample while comparing it to the baseline light transmission value [93]. A spectroradiometer is an alternative to the spectrophotometer for colour and translucency measurements as well as radiometric properties (e.g., irradiance and radiant exposure). It avoids the effects of edge loss of light by eliminating the gap between the external light source, the object, and the spectroradiometer device. When compared to the spectrophotometer, the spectroradiometer provides different translucency parameter results, but they are still highly correlated [92]. Conversely, the colorimeter device measures colour in the form of tristimulus values resulting from light reflectance of an object after the light source has passed through sequential photodiode filters, and thereby can compute colour differences between two ceramics. However, a colorimeter has many drawbacks, as they cannot measure individual spectral reflectance, are influenced by the 'edge-loss' effect of translucent materials, and light filters are sensitive to aging [88,94,95].

5.2. Translucency

Translucency of dental ceramics depends on the crystal composition, size, and distribution, the presence of pigments, and on the inherent flaw population and density. Crystals and flaws smaller than the visible-light wavelength (350–800 nm) allow complete light transmission and result in a transparent glass, while larger crystals and flaws will scatter and reflect light waves, creating a translucent ceramic. The translucency of polycrystalline ceramics is significantly impacted by the grain size and density, as light scattering occurs along the grain boundaries, thus diminishing light transmission. In order to foster translucency within polycrystalline ceramics, grain sizes are increased to reduce the grain boundaries and, in turn, lessen light scatter [96,97]. In general, translucency is considered the medium state between transparency and opacity and can be quantified by a variety of indices, including the translucency parameter, contrast ratio, and light transmittance [98,99]:

1. The translucency parameter (TP) represents the colour difference in a ceramic over ideal white (highly reflective) backgrounds and black (highly absorbent) backgrounds, and ranges between $0 < TP < 100$, wherein high TP discloses high translucency and low opacity. TP can be determined according to the CIE L*a*b* (TP_{ab}):

$$TP_{ab} = \sqrt{\left(L_B^* - L_W^*\right)^2 + \left(a_B^* - a_W^*\right)^2 + \left(b_B^* - b_W^*\right)^2} \quad (23)$$

where L^* is the measure of the lightness or darkness of the material, a^* is the measure of redness or greenness, and b^* is the measure of yellowness or blueness. Subscripts B and W refer to the colour coordinates on the black and white backgrounds, respectively [98–101]. TP can also be computed through the CIEDE2000 formula (TP_{00}):

$$TP_{00} = \sqrt{\left(\frac{L_B - L_W}{K_L S_L}\right)^2 + \left(\frac{C_B - C_W}{K_C S_C}\right)^2 + \left(\frac{\Delta H}{K_H S_H}\right)^2 + R_T\left(\frac{\Delta C}{K_C S_C}\right)\left(\frac{\Delta H}{K_H S_H}\right)} \quad (24)$$

For the TP_{ab}, the 50% PT and AT are 1.33 and 4.43, respectively, whereas for TP_{00}, the 50% PT and AT are 0.62 and 2.62, respectively [102].

2. The contrast ratio (CR) is expressed as the ratio of reflectance obtained from a ceramic against a black background to that obtained from the same ceramic against a white background. CR values range between 0 (completely transparent) and 1 (completely opaque):

$$CR = \frac{Y_b}{Y_w} \quad (25)$$

where Y_b and Y_w represent the spectral reflectance of the sample against black and white backgrounds, respectively. A significant positive correlation is found between TP and CR; thus, both can be utilised to investigate translucency [98,99].

3. Light transmittance ($T\%$). Here, translucency is computed by calculating the total light transmission through a ceramic sample. The absolute or total light transmittance is a sum of collimated (linear) and diffuse (scattered) transmitted light through the sample and its calculation factor, the reflected light; hence, it dictates using a double-beam spectrophotometer equipped with an integrating sphere with reflection standards. The apparent or direct light transmission ($T\%$) does not account for the reflected light waves and is defined as ratio of transmitted light (I_t) passing through a material to the incident light (I_0):

$$T\% = \frac{I_t}{I_0} \quad (26)$$

The human eye is most sensitive to the visible light at a 555 nm wavelength, under daylight illumination [103]; thus, the $T\%$ of dental ceramics is generally reported at 525 nm [98,104] or 550 nm [105].

5.3. Absorbance

Light absorption in dental ceramics is proportional to the amount of filler and dye particles and transpires when the energy of incident light photons is larger than that of the bandgap in atoms within the ceramic molecular structure (e.g., pigment molecules). Light photon energy is transferred to the valence band electrons (i.e., bound to the atomic structure) in pigment molecules, exciting them to cross the bandgap, thereby converting them into conduction band electrons (i.e., free to establish conduction). This excitation of electrons entails the absorption of incident light energy and is later transformed into thermal energy. Moreover, the presence of point defects within ceramic configurations, such as oxygen vacancies, can enhance light absorption and should be eliminated through adequate sintering protocols [103]. Light absorption also varies based on the wavelength (frequency) of incident light. When white light is emitted on a yellow surface, the red and green wavelengths are transmitted or reflected, whereas the blue wavelength is absorbed. Absorption ($Abs\%$) of dental ceramics can be quantified by many mathematical models, including the Kubelka–Munk theory, which measures light absorption and scattering coefficients as a function of reflectance and transmittance values, as well as the Beer–Lambert Law for light attenuation [97,106]. The latter describes the exponential rise in light

attenuation with the ceramic material thickness, and is more commonly employed due to its straightforward approach [107]:

$$Abs\% = \log\ T\% = \log \frac{I_t}{I_0} \tag{27}$$

where $T\%$ is direct light transmittance, while I_t and I_0 are transmitted and incident light intensities, respectively.

5.4. Opacity

Increased opacity of dental ceramics is considered the main cause of their aesthetic failure. While a highly opaque restoration can successfully mask underlying substrate discolorations, it also appears flat, artificial, and lifeless; thus, a harmonious balance must be achieved between the degree of opacity versus translucency of a dental ceramic [107]. The intensity of opacity is controlled by the crystalline structure, grain size, flaw distribution, thickness, and firing parameters of ceramics, as well as the colour of the underlying substrate and shade of the resin luting cement [108]. Opacity ($O\%$) is calculated as the inverse of direct light transmittance [107]:

$$O\% = T^{-1} = I_0 / I_t \tag{28}$$

5.5. Fluorescence

Fluorescence in dental ceramics is the photoluminescence that occurs in a mechanism akin to their light absorption, wherein the incident light photons with a specified wavelength are absorbed by the excited valence electrons within ceramic atoms, inciting the emission of photons with longer wavelengths. This optical property is stimulated by UV radiation as a function of exposure time: the bluish-white, fluorescent appearance of ceramics disappears when the UV source is removed. Fluorescence of ceramics is acquired by the presence of rare-earth luminescent oxides (e.g., terbium, cerium, and ytterbium) and it differs based on the ceramic composition, glass-matrix-to-crystalline ratio, colouring saturation, and sintering treatments. Exposing ceramics to repeated firing cycles reduces the fluorescence, dense crystalline frameworks alter the bluish fluorescent tint to yellow-green, and dark underlying substrates lessen the fluorescent intensity. Fluorescence can be quantified by fluorometers (spectrometers that calculate emission spectra analogous to incident light wavelengths) or fluorimeters (devices with excitation light sources that generate emission wavelengths) [109].

5.6. Opalescence

Opalescence of dental ceramics is the selective visible-light-scattering phenomenon within their translucent glass phase that arises when the mismatch between the refractive indices of crystalline and glassy phases is 1.1, thereby demonstrating blueness under reflected light spectra and orange colouring under transmitted light spectra [110]. This optical property can be quantified by the opalescence parameter (OP) computed from the ceramic colour coordinates a^* and b^* from the CIE L*a*b* colour system [98]:

$$OP = \sqrt{\left(a_B^* - a_W^*\right)^2 + \left(b_B^* - b_W^*\right)^2} \tag{29}$$

where subscripts B and W represent the colour coordinate values against black and white backgrounds, respectively.

Moreover, OP can be computed as a function of the reflected and transmitted colour coordinates, as follows:

$$OP = \sqrt{\left(a_T^* - a_R^*\right)^2 + \left(b_T^* - b_R^*\right)^2} \tag{30}$$

where subscripts *T* and *R* denote the transmitted and the reflected colour, respectively [111]. For optimum aesthetic results, ceramic restorations should exhibit similar opalescence to that of the adjacent natural dentition (*OP*: 18–22) [112].

5.7. Whiteness

Adequate measurement of the degree of whiteness is an important tool to monitor the efficacy of bleaching agents on dental ceramics. In spectral terms, a white object is defined as an object with continuous absolute (100%) light reflectance across the visible wavelength spectrum. Based on the CIE L*a*b* colour space, a white material exhibits high *L** (lightness) and low saturation. Various whiteness parameters have been implemented in the literature based on the CIE1931 XYZ tristimulus, such as the CIE whiteness index (*WIC*), ASTM whiteness index (*WI*), and the optimised whiteness index (*WIO*), while other indices are obtained from calculations as a function of the CIE L*a*b* colour space, such as the CIE whiteness (*W*) and tint (*T*) indices and CIELAB whiteness index (*WLAB*). The most recently introduced whiteness index (WI_D) was customised to measure the whiteness of dental materials and computed from the CIE L*a*b* colour space [83]. Validation tests confirmed that WI_D outperforms the previous indices in correlating with visual perception under laboratory and clinical conditions. The whiteness index (WI_D) is calculated based on *L**, *a**, and *b** colour coordinates:

$$WI_D = 0.511L^* - 2.324a^* - 1.100b^* \quad (31)$$

The PT above which 50% of observers can detect a difference between whiteness is 0.72, while the AT needed for observers to reject whiteness differences in a restoration is 2.6 [113].

5.8. Gloss

Gloss is an optical phenomenon responsible for the lustrous, mirror-like appearance of a dental ceramic, defined as the amount of spectral light reflected at a predetermined incident angle equal and opposite to its reflectance angle [114,115]. Ceramic gloss is influenced by its topography and refractive index (RI) and angle of incident light [116]. Objective gloss is recorded by a gloss meter (Figure 17) and is expressed in gloss units (*GU*; the percentage of the incident light beam/reflected light beam): 0 in an absolute nonreflective surface, and 100 in an absolute refractive surface. Based on the measured gloss of the ceramic surface, the angle of incident light is determined: 'semi-gloss' surfaces are measured at 60° and should result in *GU* values between 10 and 70. If *GU* > 70, surfaces are classified as 'high gloss' and measurements are to be repeated at 20°, and if *GU* < 10, surfaces are classified as 'matte' and gloss is remeasured at 85° [117,118].

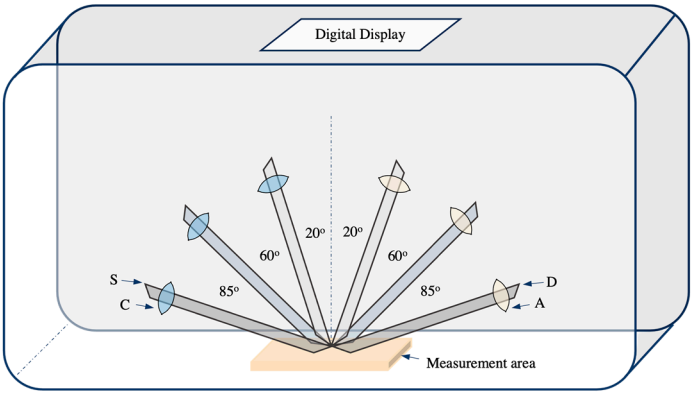

Figure 17. Schematic representation of a gloss meter with a ceramic specimen inside, where, S: source; C: collimator; A: aperture; D: detector (adapted from Fernández-Oliveras et al.) [117].

Clinically, it is essential for ceramic materials to exhibit similar gloss values to enamel ($40 < GU < 52$); therefore, the acceptable gloss of dental ceramics should be $40 < GU < 60$ [119]. The PT above which 50% of observers can detect gloss differences is $\Delta GU = 6.4$, while the AT needed for observers to reject gloss differences in a restoration is $\Delta GU = 35.7$. Subjective gloss perception in the clinic is controlled by the type of illuminant, angle of visualisation, colour of the background, observer education level, as well as the restoration geometry and texture [120].

5.9. Transmitted Irradiance

Light-curing units (LCUs) have become increasingly popular tools in alliance with the popularity of resin-based luting agents used to adhesively cement ceramic restorations [121]. Interpretation of properties and threshold requirements related to light-curing units (LCUs) is enabled through precise understanding of scientific terminology in accordance with the International System of Units and the EN ISO 10650:2018 standards [122,123]. Radiant power (mW) is the LCU energy emitted per unit of time, while radiant exitance (mW/cm^2) is the radiant power emitted from the light-curing surface. Thus, LCUs with equal radiant power may differ in their radiant exitance depending on the LCU tip area, i.e., higher radiant energy transpires when the tip area is reduced. Moreover, LCU radiant exitance within the 380–515 nm wavelength range should not exceed 4000 mW/cm^2. Irradiance (mW/cm^2) is the radiant power obtained by a unit area of a dental material and is equivalent to the radiant emittance when there is zero distance between an LCU and the underlying material. Radiant exposure (J/cm^2) is the energy received per unit area of a dental material, wherein 2 mm resin composite increments require 16 J/cm^2 in order to complete polymerisation. Moreover, an inverse relationship has been proven between the ceramic substrate thickness and the transmitted irradiance to the underlying resin luting cement [124]. Identification of LCU radiant power, radiant exposure, delivered irradiance, and interposing distances is of utmost importance in understanding the implications on photocured resin cements [122,125]. A schematic diagram of the components of a poly-wave LED LCU is presented in Figure 18, highlighting the differences between LED-related properties and the photocured substrate-related properties.

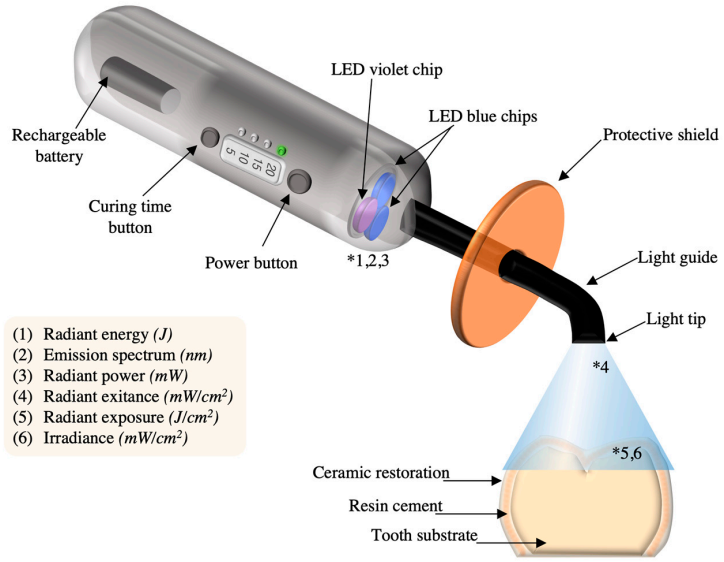

Figure 18. Schematic diagram of poly-wave LED LCU, with highlighted properties (*) pertaining to the LCU or the substrate. Note: location of LED chips could differ among commercial LED LCUs, either located within the LCU body (as shown) or within the curing tip [126].

Multiple methods have been utilised to measure radiant exposure and irradiance received on the top surfaces of restorative dental materials, such as radiometers, cosine,

integrating spheres, and spectrometers. A benchtop calibrated radiometer customised to quantify the radiant exposure, radiant power, and delivered irradiance from LCUs is the Managing Accurate Resin Curing System Light Collector, MARC-LC™ (Bluelight Analytics Inc., Halifax, NS, Canada; Figure 19) [127]. MARC-LC™ is a calibrated radiometer comprised of top and bottom sensors with cosine correctors (i.e., optical diffusers coupled to collect light from a 180° view field). Sensors are connected via a bifurcated fibre optic cable to a spectrometer (Model USB4000, Ocean Optics Inc., Dunedin, FL, USA) that enables the device to record the LCU-delivered irradiance received at the top and bottom of a dental material throughout the duration of radiation time. The LCU is held in its desired position in relation to the MARC-LC™ sensors by means of adjustable accessory arms and knobs that regulate its horizontal and vertical movements. Upon initiating the light-curing cycle, the energy output is instantaneously recorded by the spectrometer and transferred to a pre-formatted computer with custom software (MARCTM, Bluelight Analytics Inc., Halifax, NS, Canada) that collects, stores, and exports data measurements, including the actual curing time, radiant exposure, emission spectrum, and average and maximum irradiance and radiant power values. The MARC-LC™ system surpassed its predecessor (Managing Accurate Resin Curing System-Resin Calibrator, MARC-RC®), as measurements acquired by the former encompass the entire light-emitting tip (∅ = 16 mm), while the latter obtains measurements from the innermost 4 mm diameter of the tip [127–129].

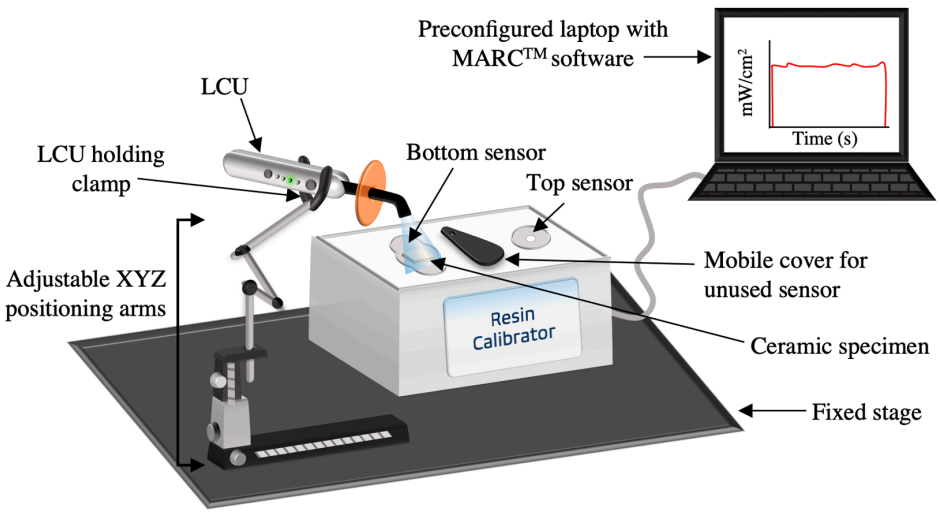

Figure 19. Schematic diagram of the MARC-LC™ radiometer in conjunction with a LUC and ceramic substrate.

5.10. Research Trends in Spectrophotometric Characterisation of Dental Ceramics

Perceptibility and acceptability thresholds are essential objective approaches that aid in guiding clinical decision-making, especially when dealing with patients with high aesthetic expectations. Colorimetric analysis of dental ceramics using the CIELAB system is highly beneficial in determining their degree of stainability as well as shade-matching ceramic restorations to the adjacent natural dentition. Nonetheless, there are multidimensional factors that impact the spectrophotometric devices' capacity in accurately recording colour coordinates of dental ceramics, such as specimen surface texture, surrounding and background colour, aperture size, illuminate type, and degree of light incidence. These factors should be taken into consideration when comparing colour-related findings pertaining to dental ceramics in the literature [98,130].

6. Microstructural Characterisation

Microstructural analysis is imperative owing to the existing differences in chemical composition, microstructure, and crystallinity of dental ceramics. Furthermore, ceramic restorations are exposed to a variety of surface treatments that alter the underlying morpho-

logical framework: intaglio surfaces are acid-etched or sandblasted, and external surfaces are exposed to differing polishing, glazing, and staining protocols. Bearing in mind the multitude of recently introduced ceramic surface treatment modalities, such as silicatisation, 10 MPD coating, laser irradiation, and plasma application, there is a need to understand their novel mechanisms at a microscopic level.

6.1. Scanning Electron Microscope

The scanning electron microscope (SEM) is a multipurpose, high-resolution imaging tool that provides qualitative and quantitative analysis of material morphology, composition, and fractographic patterns of dental ceramics. SEM has a large depth of field, thereby permitting a wider scanning area in focus at high levels of resolution (1–2 nm) and magnification (10×–500k×). Images are generated as a function of a high-energy condensed electron beam emitted from the cathode (e.g., field emission electron gun and tungsten filament), which passes through a sequence of electromagnetic lenses and apertures within a vacuum column until it hits the ceramic specimen (Figure 20). Subsequently, the electrons interact with the atoms on the material surface, inciting the specimen to eject secondary electrons (SE) and backscattered electrons (BSE) that are collected by SE and BSE detectors, respectively, to be converted into signals that form the magnified image on the associated device screen. SE are released from superficial areas of the specimen and deliver qualitative data, including morphology and fractographic patterns. Conversely, BSE are emitted from the deeper specimen zones, and thus communicate quantitative chemical analysis. Ceramic specimens are commonly coated with thin metallic films (e.g., gold and palladium) to enhance their electrical conductivity and render sharper SEM images; however, when low acceleration voltages and decreased aperture sizes are implemented, accurate images can be obtained without conductive coating. Furthermore, SEM is often supplemented with energy-dispersive spectroscopy (EDS), which utilises X-rays unique to each chemical element, and can thereby pinpoint specific elements in samples and quantify their elemental concentrations. Localised elemental analysis by EDS can deliver insight about the presence of second-phase grains, inclusions, and contaminants within ceramic structures [131,132].

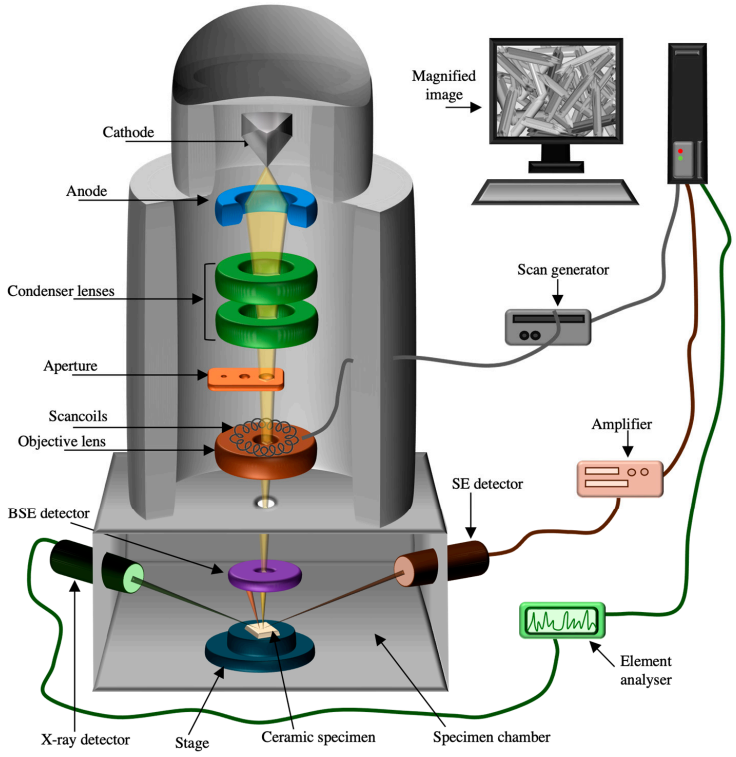

Figure 20. Schematic diagram of SEM components (BSE: backscattered electrons and SE: secondary electrons).

6.2. X-ray Diffraction

X-ray diffraction (XRD) is a valuable, non-destructive method that can be employed to characterise dental ceramics by delivering information on their crystalline structures, orientations, atomic spacing, and phases, as well as grain sizes, micro-strains, and dislocation densities, based on the interactions between incident X-rays and the crystals within ceramic specimens. X-rays are emitted at high voltages from a cathode (heated filament), collimated into a condensed monochromatic beam, and targeted at the crystals within superficial layers of a ceramic sample (10 µm–1 mm depth; Figure 21). Upon interacting with these radiations, ceramic crystals diffract X-rays at unique angles and intensities related to their crystal lattice planes and atomic distributions, i.e., the X-ray is diffracted when its wavelength is equivalent to the crystal interatomic spacing, in accordance with Bragg's Law [133]:

$$n\lambda = 2d \sin \theta \quad (32)$$

where n is an integer (1, 2. . .n), λ is the emitted X-ray wavelength, d is interatomic space, and θ is the angle of incidence.

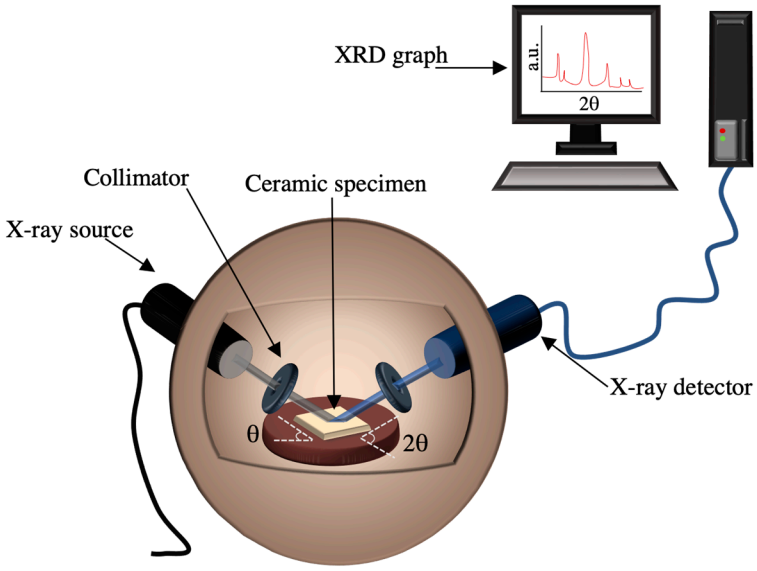

Figure 21. Illustrative diagram depicting XRD components.

Diffracted X-ray peaks are detected by an X-ray detector, analysed, quantified, and converted to d-spacings, which are compared to standard reference databases and matched with individual crystal components [133]. XRD data are collected at the 2θ° angle rotating X-ray detector, i.e., angle between transmitted and diffracted beams, instead of θ° (angle between the diffracted beam and imperceptible crystal plane).

Quantitative analysis by XRD was obtained through Rietveld refinement and the Scherrer equation [134] to calculate crystallite sizes from the width of diffraction peaks correspondent to crystalline phases:

$$D = k\lambda / B cos\theta \quad (33)$$

where D is the crystallite size, k is a geometrical constant (0.89), λ is the wavelength of the X-ray, B is the full width at half maximum of the diffraction peak, and θ is the incident angle.

Nonetheless, in the case of dental ceramics comprised of an amorphous glass phase, an overestimation of the crystal content could result from Rietveld refinement. In such ceramics, the G-factor is employed for absolute quantification of crystalline and residual glass phases, in which quartzite is used as the external standard [135]. The G-factor is computed as follows:

$$G = S_q \left[\left(\rho_q V_q^2 \mu_q^* \right) / c_q \right] \quad (34)$$

where S_q is the Rietveld scale factor of quartz, ρ_q is the quartz density, V_q is the quartz unit-cell volume, and μ_q* is the quartzite mass attenuation coefficient. S_q, ρ_q, and V_q are obtained from the Rietveld refinement of the quartz in quartzite and μ_q^* is derived from calculating the mass attenuation coefficients of quartzite elements obtained from the International Tables for Crystallography [136].

Thereafter, the quantity of crystalline phases (c_j) within a dental glass ceramic is computed as follows:

$$c_j = S_j\left[\left(\rho_j V_j^2 \mu_{sample}^*\right)/G\right] \quad (35)$$

where S_j is the crystalline phase Rietveld scale factor, ρ_j is the crystalline phase density, V_j is the crystal phase unit-cell volume acquired from its Rietveld refinement, μ_{sample}^* is the mass attenuation coefficient of the sample (obtained from X-ray fluorescence and inductive coupled plasma optical emission spectroscopy), and G is the G-factor. Consequently, the absolute amorphous content is the remaining percentage of all the total quantified crystalline phases yielding 100 wt% [27].

6.3. X-ray Fluorescence

X-ray fluorescence analysis (XRF) is a useful, non-destructive analytical tool in which high-energy X-ray irradiation is focused onto dental ceramic specimens, resulting in the excitation of a fluorescent X-ray emission, which is correspondent to the elemental composition (Figure 22). Considering that XRF can be executed in air, there is no need for a vacuumed specimen chamber, and there is also no prerequisite for surface treatment of a ceramic specimen, such as fixation, dehydration, or coating with an electroconductive substance. XRF can tolerate small sized specimens in the form of powders, pastes, solids, or even liquids. Furthermore, it can detect trace amounts of a vast range of elements with low excitation potential within a penetration depth of 0.5–3 µm. Nonetheless, there are certain light elements that cannot be identified through this technique, including lithium, beryllium, sodium, magnesium, aluminium, silicon, and phosphorus [137,138]. Thereby, XRF is commonly coupled with inductively coupled plasma optical emission spectroscopy (ICP-OES) for the detection of such elements [27].

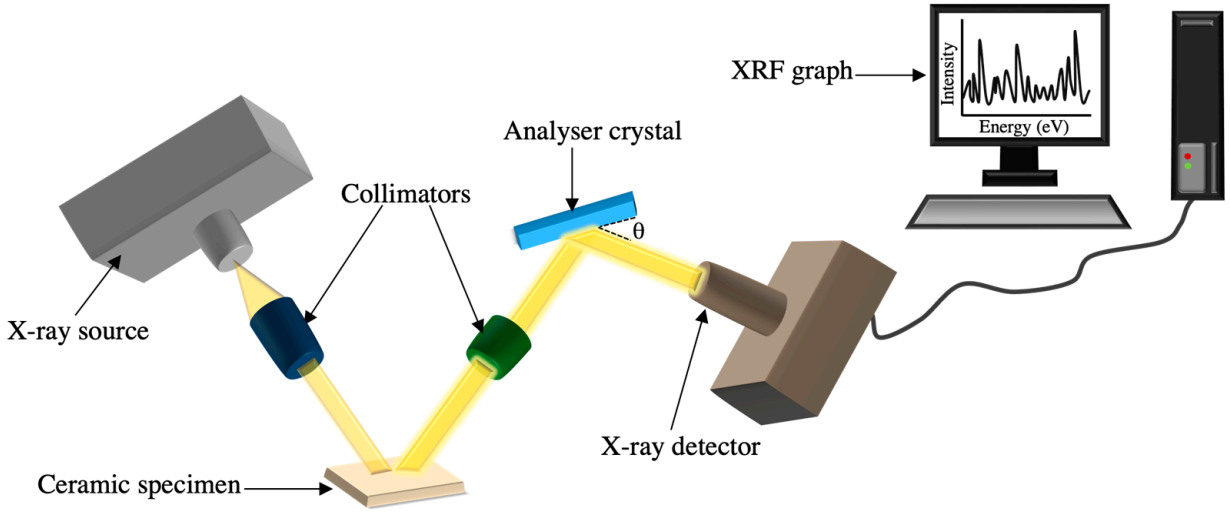

Figure 22. Schematic diagram illustrating XRF components.

6.4. X-ray Photoelectron Spectroscopy

X-ray photoelectron spectroscopy (XPS) can provide information regarding the identification and quantification of chemical elements within the most superficial layers (<10 nm) of dental ceramics by computing the kinetic energy of electrons emitted from the ceramic as a function of X-ray excitation. A probe beam of mono-energetic X-rays is employed to irradiate a ceramic specimen, exciting the specimen surface electrons residing in multi-orbital

levels, causing them to gain kinetic energy and, in turn, be emitted from the specimen surface. Subsequently, the kinetic energy of the emitted electron is detected and converted into an XPS spectra specific for each constituting element based on the specific binding energy (eV) peaks corresponding to each electron orbital (Figure 23). While XPS can detect almost all periodic elements, it cannot identify elements with absent core electrons (e.g., hydrogen and helium). Another significant limitation in this method is its high sensitivity to surface contamination (i.e., carbon contamination) [138,139].

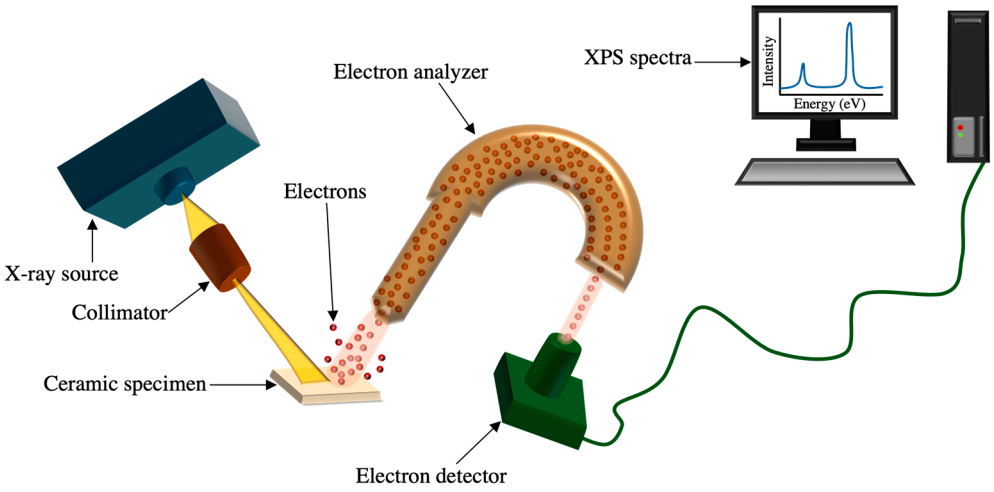

Figure 23. Schematic illustration of the XPS device.

6.5. Fourier Transform Infrared Spectroscopy

Fourier transform infrared spectroscopy (FTIR) employs an electromagnetic infrared spectrum within a wavenumber (i.e., waves per cm) ranging between 14,000 and 200 cm^{-1} and can be used to assess dental ceramics. Upon energy absorption, the chemical bonds within ceramic molecules undergo vibration, and an absorption spectrum can be acquired by plotting transmitted or absorbed radiation against the wavenumber. FTIR aids in the identification of functional groups and organic, polymeric, and, to a lesser degree, inorganic compounds, as well as information regarding atomic interactions and compound purity residing within a penetration depth of 0.5–3 µm. This method is fairly straightforward and can be utilised on gaseous, liquid, and solid matters in a relatively short amount of time [138,140].

6.6. Raman Spectroscopy

Incident monochromatic radiation is scattered by the component molecules of dental ceramic specimens at specific frequencies, either similar to that of the incident light (Rayleigh scattering) or different (Raman scattering). In the latter, the 'Raman shift' is determined as the difference between the incident and scattered radiation frequencies. Raman spectra are obtained as a function of the intensity of the scattered light versus the wavenumber (cm^{-1}), where the intensity of the radiation is correlated with the molar concentration and thickness of the layer. This technique can be utilised to identify compounds, phases, and phase transformations within ceramic materials residing within a depth of 0.01–2300 µm [138,141,142].

6.7. Research Trends in Microstructural Characterisation of Dental Ceramics

The appropriate selection of microstructural characterisation approaches is governed by a variety of factors, such as the penetration depth, elemental detection capacity, and the physical state of ceramic materials (solid, powder, liquid, etc.). As verified from the diverse methodologies mentioned above, there are significant benefits to be reaped from compositional and crystallographic observations of dental ceramics. Nonetheless,

qualitative analysis is fundamentally complementary to quantitative investigations, as both are essential to obtain a comprehensive understanding of ceramic material's functional behaviour and fractographic patterns.

7. Thermal Characterisation

Dental glass ceramics are manufactured through meticulous and slow temperature-controlled heating of precursor (parent) glasses. In order to yield homogeneity within the precursor glass, the molten raw glass products are simultaneously melted beyond their liquidus temperature, then quenched below their glass transition temperature at a rate (q) faster than the critical cooling rate (q_c) to eliminate premature nucleation. Subsequently, the parent glass is heated to initiate nucleation, followed by crystal formation and growth. Owing to the thermally dependent dimensional behaviour of ceramics, dedicated thermal analytical methods are beneficial in investigating the ceramic thermal stability and solid/liquid phase transitions. A variety of material-specific thermal parameters can be identified: glass transition temperature, T_g (solid glass transformation to rubbery supercooled liquid), nucleation temperature, T_n, crystallisation temperature, T_c, melting temperature, T_m (melting onset), liquidus temperature, T_L (melting endpoint), and thermal expansion [51,143,144].

7.1. Differential Scanning Calorimetry and Differential Thermal Analysis

Differential scanning calorimetry (DSC) is a thermo-analytical apparatus used to quantify the heat required to raise the temperature of a ceramic specimen needed to illicit phase transformation as a function of time and temperature. DSC software generates thermographs that illustrate onset, peak, and termination temperatures corresponding to intrinsic endothermic and exothermic processes of phase transformation as well as enthalpy and entropy changes [144,145]. The differential thermal analysis (DTA) mechanism resembles that of the DSC; however, the former differs in regard to reporting the phase transformations as a function of the change in temperature (ΔT) instead of the heat flow values reported by the latter (Figure 24) [145].

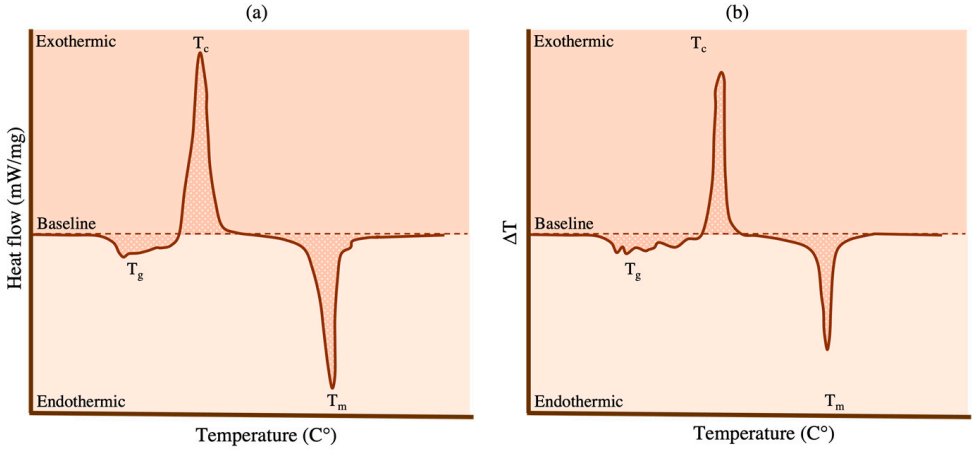

Figure 24. Schematic diagram of a (**a**) DSC curve and (**b**) DTA curve illustrating thermal dental ceramic behaviour.

7.2. Thermogravimetric Analysis

Firing and cooling of dental ceramics impact their dimensional stability due to water loss/uptake, elemental volatilisation, and oxidation. Thermogravimetric analysis (TGA) quantifies the percentage of mass change (wt %) that takes place upon heating dental ceramics as a function of temperature or time. Testing conditions can be adjusted in terms of thermal parameters (fixed heating rate or fixed temperatures) or atmospheric conditions (inert, reactive, or oxidising), and concurrent DSC or DTA measurements can be reported [145].

7.3. Thermal Dilatometry

According to ISO standard 9693:2019 [4], thermal compatibility in veneers can be predicted from individual veneering and substrate materials' coefficients of linear thermal expansion (CTE). CTE depicts the rate of elongation (μm) corresponding to the increase in temperature (C°), with the assumption of a linear relationship between both factors. CTE of dental ceramics can be computed via vertical or horizontal pushrod dilatometers equipped with strain sensors and a thermocouple (Figure 25) [143].

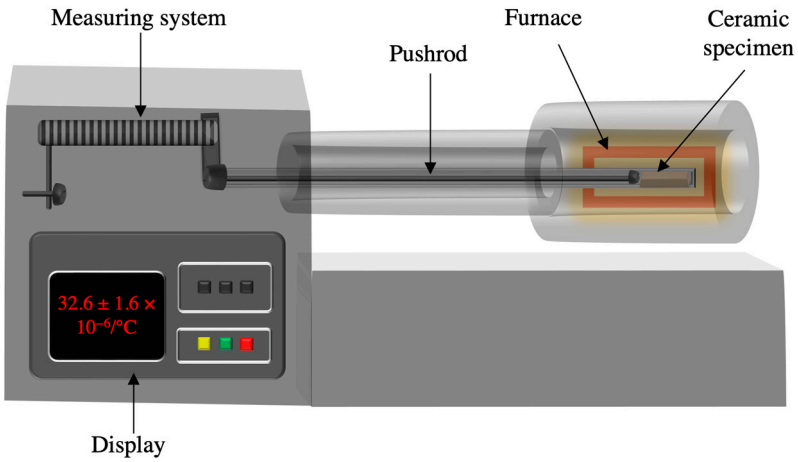

Figure 25. Schematic diagram of the horizontal pushrod dilatometer.

7.4. Research Trends in Thermal Characterisation of Dental Ceramics

In terms of the material engineering sector, thermal investigations can provide substantial data needed for tailoring and optimising the optical and mechanical properties of dental ceramics, through meticulously controlled heat refinement regimens. Regulation of the nucleation rate has shown to determine the nature of nucleation (heterogenous versus homogenous nucleation), which in turn impacts the resultant crystallisation mode (surface versus volume crystallisation), thus considerably influencing the microstructure and, accordingly, the mechanical performance of dental ceramics [51]. Among the advantages of thermal analysis methods are their relative straightforwardness, their tolerance to miniature-sized sample dimensions, as well as to solid and liquid specimens, and the ability to collect observations over a wide range of temperatures. Moreover, the differential scanning calorimetry heat flow curves verified that the glass transition and melting temperatures of dental ceramics demonstrate an inverse relationship to their firing temperature. This knowledge—in addition to the coefficient of linear thermal expansion data—can aid in predicting dental ceramics' potential employment as veneers to underlying ceramic or metallic substrates. Nevertheless, certain limitations persist within individual techniques, such as the overlapping of phase transition peaks in differential scanning calorimetry and differential thermal analysis, causing difficulty in data interpretation and an inability to differentiate between samples of similar thermal processes. Furthermore, thermogravimetric analysis cannot identify changes within dental ceramic samples unless they are accompanied by a change in mass; thus, samples that do not exhibit a weight change cannot be analysed by this particular method [145].

8. Discussion and Conclusions

Current trends in dental ceramics laboratory testing are substantially leaning towards clinically relevant methodologies to accurately simulate underlying intraoral mechanisms. Driven by the current popularity of subtractive manufacturing and the proven success of CAD/CAM ceramic prostheses, recently introduced ISO standards are aimed at investigating machinable ceramics intended for the fabrication of dental fixed restorations. This review summarised the multi-fold characterisation modalities (mechanical, tribological,

topographical, spectrophotometric, microstructural, and thermal) employed to translate the performance of dental ceramics into quantifiable values and, where appropriate, the required thresholds pertaining to clinical indications have been reported. Nonetheless, the aforementioned methodologies in this review are by no means a summation of ceramic-related testing approaches, but rather a structured outline of popular characterisation modalities as well as an in-depth discussion of recently introduced characterisation approaches, such as the ball-on-three-balls flexural strength test and the merlon fracture test. An array of characterisation parameters relating to dental ceramics have not been discussed at present due to lengthwise confines of the review format. These include, but are not limited to, the impact strength test, slow crack growth parameter, fatigue resistance test, and finite element analysis. Furthermore, when designing future research models, it is crucial to confirm that specific testing assumptions are met and correct geometric requirements are maintained in order to ensure accurate data interpretation. Care must be taken by dental practitioners in correctly understanding the appropriate terminology relating to dental ceramics to avoid misinterpretation of existing scientific literature and to prevent misleading overestimation of newly marketed commercial dental products.

Author Contributions: Conceptualisation, methodology, software, investigation, resources, data curation, writing—original draft preparation, H.A.-J.; validation and formal analysis, H.A.-J., J.H. and M.B.; writing—review and editing, J.H., M.B., N.S. and J.S.; supervision, N.S. and J.S.; project administration and funding acquisition, H.A.-J. All authors have read and agreed to the published version of the manuscript.

Funding: This research was funded by the Saudi Arabian Cultural Bureau in London, UK through a full-time scholarship for the first author, Hanan Al-Johani. The funder had no role in the study design, data collection and analysis, decision to publish, or preparation of the manuscript.

Institutional Review Board Statement: Not applicable.

Informed Consent Statement: Not applicable.

Data Availability Statement: The data presented in this study are available upon request from the corresponding author.

Conflicts of Interest: The authors declare no conflicts of interest.

References

1. Lohbauer, U.; Belli, R. *Dental Ceramics: Fracture Mechanics and Engineering Design*; Springer Nature: Cham, Switzerland, 2022.
2. *BS EN ISO 18675:2022*; Dental-Machinable Ceramic Blank. International Organization for Standardization: Geneva, Switzerland, 2022.
3. *BS EN ISO 6872:2023*; Dentistry—Ceramic Materials. International Organization for Standardization: Geneva, Switzerland, 2023.
4. *BS EN ISO 9693:2019*; Dentistry—Compatibility Testing for Metal-Ceramic and Ceramic-Ceramic Systems. International Organization for Standardization: Geneva, Switzerland, 2019.
5. Sakaguchi, R.L.; Ferracane, J.; Powers, J.M. *Craig's Restorative Dental Materials-e-Book*, 14th ed.; Elsevier Health Sciences: Amsterdam, The Netherlands, 2019.
6. Xu, Y.; Han, J.; Lin, H.; An, L. Comparative study of flexural strength test methods on CAD/CAM Y-TZP dental ceramics. *Regen. Biomater.* **2015**, *2*, 239–244. [CrossRef] [PubMed]
7. Hooshmand, T.; Parvizi, S.; Keshvad, A. Effect of surface acid etching on the biaxial flexural strength of two hot-pressed glass ceramics. *J. Prosthodont.* **2008**, *17*, 415–419. [CrossRef] [PubMed]
8. Wendler, M.; Belli, R.; Petschelt, A.; Mevec, D.; Harrer, W.; Lube, T.; Danzer, R.; Lohbauer, U. Chairside CAD/CAM materials. Part 2: Flexural strength testing. *Dent. Mater.* **2017**, *33*, 99–109. [CrossRef] [PubMed]
9. Lube, T.; Manner, M.; Danzer, R. The Miniaturisation of the 4-Point-Bend Test. *Fatigue. Fract. Eng. Mater. Struct.* **1997**, *20*, 1605–1616. [CrossRef]
10. Börger, A.; Supancic, P.; Danzer, R. The ball on three balls test for strength testing of brittle discs: Stress distribution in the disc. *J. Eur. Ceram. Soc.* **2002**, *22*, 1425–1436. [CrossRef]
11. Danzer, R.; Harrer, W.; Supancic, P.; Lube, T.; Wang, Z.; Börger, A. The ball on three balls test—Strength and failure analysis of different materials. *J. Eur. Ceram. Soc.* **2007**, *27*, 1481–1485. [CrossRef]
12. Börger, A.; Supancic, P.; Danzer, R. The ball on three balls test for strength testing of brittle discs: Part II: Analysis of possible errors in the strength determination. *J. Eur. Ceram. Soc.* **2004**, *24*, 2917–2928. [CrossRef]
13. Wiskott, H.W.; Nicholls, J.I.; Belser, U.C. Stress fatigue: Basic principles and prosthodontic implications. *Int. J. Prosthodont.* **1995**, *8*, 105–116.

14. *EN 843-5*; Advanced Technical Ceramics, Monolithic Ceramics, Mechanical Properties at Room Temperature, Part 5: Statistical Analysis. European Committee for Standardization: Brussels, Belgium, 2007.
15. Quinn, J.B.; Quinn, G.D. A practical and systematic review of Weibull statistics for reporting strengths of dental materials. *Dent. Mater.* **2010**, *26*, 135–147. [CrossRef]
16. *BS EN ISO 20501:2022*; Fine Ceramics (Advanced Ceramics, Advanced Technical Ceramics). Weibull Statistics for Strength Data, International Organization for Standardization: Geneva, Switzerland, 2022.
17. Harrer, W.; Danzer, R.; Supancic, P.; Lube, T. The ball on three balls test: Strength testing of specimens of different sizes and geometries. In Proceedings of the 10th International Conference of the European Ceramic Society, Berlin, Germany, 17–21 June 2007; pp. 1271–1275.
18. Quinn, G.D. Weibull strength scaling for standardized rectangular flexure specimens. *J. Am. Ceram. Soc.* **2003**, *86*, 508–510. [CrossRef]
19. Alkadi, L.; Ruse, N.D. Fracture toughness of two lithium disilicate dental glass ceramics. *J. Prosthet. Dent.* **2016**, *116*, 591–596. [CrossRef] [PubMed]
20. Ilie, N.; Hickel, R.; Valceanu, A.S.; Huth, K.C. Fracture toughness of dental restorative materials. *Clin. Oral Investig.* **2012**, *16*, 489–498. [CrossRef]
21. Soderholm, K.J. Review of the fracture toughness approach. *Dent. Mater.* **2010**, *26*, e63–e77. [CrossRef]
22. Ruse, N.D. Fracture mechanics characterization of dental biomaterials. In *Dental Biomaterials*; Woodhead Publishing: Cambridge, UK, 2008.
23. Ruse, N.D.; Troczynski, T.; MacEntee, M.I.; Feduik, D. Novel fracture toughness test using a notchless triangular prism (NTP) specimen. *J. Biomed. Mater. Res.* **1996**, *31*, 457–463. [CrossRef]
24. Žmak, I.; Ćorić, D.; Mandić, V.; Ćurković, L. Hardness and Indentation Fracture Toughness of Slip Cast Alumina and Alumina-Zirconia Ceramics. *Materials* **2019**, *13*, 122. [CrossRef]
25. Scherrer, S.S.; Denry, I.L.; Wiskott, H.W. Comparison of three fracture toughness testing techniques using a dental glass and a dental ceramic. *Dent. Mater.* **1998**, *14*, 246–255. [CrossRef] [PubMed]
26. Fischer, H.; Marx, R. Fracture toughness of dental ceramics: Comparison of bending and indentation method. *Dent. Mater.* **2002**, *18*, 12–19. [CrossRef] [PubMed]
27. Lubauer, J.; Belli, R.; Peterlik, H.; Hurle, K.; Lohbauer, U. Grasping the Lithium hype: Insights into modern dental Lithium Silicate glass-ceramics. *Dent. Mater.* **2022**, *38*, 318–332. [CrossRef]
28. Lube, T.; Rasche, S.; Nindhia, T.G.T. A fracture toughness test using the ball-on-three-balls test. *J. Am. Ceram. Soc.* **2016**, *99*, 249–256. [CrossRef]
29. Belli, R.; Wendler, M.; Petschelt, A.; Lube, T.; Lohbauer, U. Fracture toughness testing of biomedical ceramic-based materials using beams, plates and discs. *J. Eur. Ceram. Soc.* **2018**, *38*, 5533–5544. [CrossRef]
30. Strobl, S.; Rasche, S.; Krautgasser, C.; Sharova, E.; Lube, T. Fracture toughness testing of small ceramic discs and plates. *J. Eur. Ceram. Soc.* **2014**, *34*, 1637–1642. [CrossRef]
31. Lubauer, J.; Ast, J.; Göken, M.; Merle, B.; Lohbauer, U.; Belli, R. Resistance-curve envelopes for dental lithium disilicate glass-ceramics. *J. Eur. Ceram. Soc.* **2022**, *42*, 2516–2522. [CrossRef]
32. Lubauer, J.; Lohbauer, U.; Belli, R. Fatigue Threshold R-Curves for Dental Lithium Disilicate Glass-Ceramics. *J. Dent. Res.* **2023**, *102*, 1106–1113. [CrossRef] [PubMed]
33. Song, X.-F.; Ma, H.-R.; He, Y.-P.; Yin, L. Soft machining-induced surface and edge chipping damage in pre-crystalized lithium silicate glass ceramics. *J. Mech. Behav. Biomed. Mater.* **2022**, *131*, 105224. [CrossRef]
34. Chen, X.-P.; Xiang, Z.-X.; Song, X.-F.; Yin, L. Machinability: Zirconia-reinforced lithium silicate glass ceramic versus lithium disilicate glass ceramic. *J. Mech. Behav. Biomed. Mater.* **2020**, *101*, 103435. [CrossRef] [PubMed]
35. Jeong, C.-S.; Moon, J.-M.; Lee, H.-J.; Bae, J.-M.; Choi, E.-J.; Kim, S.-T.; Park, Y.; Oh, S. Evaluation of the machinability and machining accuracy of polymer-based CAD/CAM blocks using merlon fracture test model. *Dent. Mater. J.* **2023**, *42*, 273–281. [CrossRef]
36. Boccaccini, A. Machinability and brittleness of glass-ceramics. *J. Mater. Process. Technol.* **1997**, *65*, 302–304. [CrossRef]
37. Lawn, B.; Marshall, D. Hardness, toughness, and brittleness: An indentation analysis. *J. Am. Ceram. Soc.* **1979**, *62*, 347–350. [CrossRef]
38. Juri, A.Z.; Belli, R.; Lohbauer, U.; Ebendorff-Heidepriem, H.; Yin, L. Edge chipping damage in lithium silicate glass-ceramics induced by conventional and ultrasonic vibration-assisted diamond machining. *Dent. Mater.* **2023**, *39*, 557–567. [CrossRef]
39. Quinn, J.; Quinn, G. Indentation brittleness of ceramics: A fresh approach. *J. Mater. Sci.* **1997**, *32*, 4331–4346. [CrossRef]
40. Brandeburski, S.B.N.; Vidal, M.L.; Collares, K.; Zhang, Y.; Della Bona, A. Edge chipping test in dentistry: A comprehensive review. *Dent. Mater.* **2020**, *36*, e74–e84. [CrossRef]
41. Pfeilschifter, M.; Preis, V.; Behr, M.; Rosentritt, M. Edge strength of CAD/CAM materials. *J. Dent.* **2018**, *74*, 95–100. [CrossRef]
42. Shen, C.; Rawls, H.R.; Esquivel-Upshaw, J.F. *Phillips' Science of Dental Materials*, 13th ed.; Elsevier: Amsterdam, The Netherlands, 2022.
43. Ilie, N.; Hilton, T.J.; Heintze, S.D.; Hickel, R.; Watts, D.C.; Silikas, N.; Stansbury, J.W.; Cadenaro, M.; Ferracane, J.L. Academy of Dental Materials guidance-Resin composites: Part I-Mechanical properties. *Dent. Mater.* **2017**, *33*, 880–894. [CrossRef]
44. Darvell, B.W. *Materials Science for Dentistry*, 10th ed.; Elsevier Mosby: Philadelphia, PA, USA, 2018.

45. Westrich, R.M. *Use of the Scanning Electron Microscope in Microhardness Testing of High-Hardness Materials*; American Society for Testing and Materials International: West Conshohocken, PA, USA, 1985.
46. Shahdad, S.A.; McCabe, J.F.; Bull, S.; Rusby, S.; Wassell, R.W. Hardness measured with traditional Vickers and Martens hardness methods. *Dent. Mater.* **2007**, *23*, 1079–1085. [CrossRef] [PubMed]
47. Samuels, L.E. *Microindentations in Metals*; ASTM STP: Philadelphia, PA, USA, 1986.
48. Fischer, J.; Roeske, S.; Stawarczyk, B.; Hämmerle, C.H. Investigations in the correlation between Martens hardness and flexural strength of composite resin restorative materials. *Dent. Mater. J.* **2010**, *29*, 188–192. [CrossRef] [PubMed]
49. Bhushan, B. *Modern Tribology Handbook*; CRC Press: Boca Raton, FL, USA, 2001.
50. Hampe, R.; Lümkemann, N.; Sener, B.; Stawarczyk, B. The effect of artificial aging on Martens hardness and indentation modulus of different dental CAD/CAM restorative materials. *J. Mech. Behav. Biomed. Mater.* **2018**, *86*, 191–198. [CrossRef]
51. Lohbauer, U.; Fabris, D.C.N.; Lubauer, J.; Abdelmaseh, S.; Cicconi, M.-R.; Hurle, K.; de Ligny, D.; Goetz-Neunhoeffer, F.; Belli, R. Glass science behind lithium silicate glass-ceramics. *Dent. Mater.* **2024**, *40*, 842–857. [CrossRef] [PubMed]
52. *ISO/TS 14569-1:2007*; Dental Materials—Guidance on Testing of Wear—Part 1: Wear by Toothbrushing. International Organization for Standardization: Geneva, Switzerland, 2007.
53. *ISO/TS 14569-2:2001*; Dental Materials—Guidance on Testing of Wear—Part 2: Wear by Two- and/or Three Body Contact. International Organization for Standardization: Geneva, Switzerland, 2001.
54. Lanza, A.; Ruggiero, A.; Sbordone, L. Tribology and Dentistry: A Commentary. *Lubricants* **2019**, *7*, 52. [CrossRef]
55. Carvalho, A.; Pinto, P.; Madeira, S.; Silva, F.S.; Carvalho, O.; Gomes, J.R. Tribological characterization of dental restorative materials. *Biotribology* **2020**, *23*, 100140. [CrossRef]
56. Santos, M.; Coelho, A.S.; Paula, A.B.; Marto, C.M.; Amaro, I.; Saraiva, J.; Marques Ferreira, M.; Antunes, P.; Carrilho, E. Mechanical and tribological characterization of a dental ceromer. *J. Funct. Biomater.* **2020**, *11*, 11. [CrossRef]
57. Wang, R.; Zhu, Y.; Chen, C.; Han, Y.; Zhou, H. Tooth Wear and Tribological Investigations in Dentistry. *Appl. Bionics Biomech.* **2022**, *2022*, 2861197. [CrossRef] [PubMed]
58. Patil, A.; D, D.J.; Bomze, D.; Gopal, V. Wear behaviour of lithography ceramic manufactured dental zirconia. *BMC Oral Health* **2023**, *23*, 276. [CrossRef]
59. Borrero-Lopez, O.; Guiberteau, F.; Zhang, Y.; Lawn, B.R. Wear of ceramic-based dental materials. *J. Mech. Behav. Biomed. Mater.* **2019**, *92*, 144–151. [CrossRef] [PubMed]
60. Hawsawi, R.A.; Miller, C.A.; Moorehead, R.D.; Stokes, C.W. Evaluation of reproducibility of the chemical solubility of dental ceramics using ISO 6872:2015. *J. Prosthet. Dent.* **2020**, *124*, 230–236. [CrossRef] [PubMed]
61. Soriano-Valero, S.; Román-Rodriguez, J.L.; Agustín-Panadero, R.; Bellot-Arcís, C.; Fons-Font, A.; Fernández-Estevan, L. Systematic review of chewing simulators: Reality and reproducibility of in vitro studies. *J. Clin. Exp. Dent.* **2020**, *12*, e1189–e1195. [CrossRef]
62. Zheng, Y.; Bashandeh, K.; Shakil, A.; Jha, S.; Polycarpou, A.A. Review of dental tribology: Current status and challenges. *Tribol. Int.* **2022**, *166*, 107354. [CrossRef]
63. Bollen, C.M.; Papaioanno, W.; Van Eldere, J.; Schepers, E.; Quirynen, M.; Van Steenberghe, D. The influence of abutment surface roughness on plaque accumulation and peri-implant mucositis. *Clin. Oral Implants Res.* **1996**, *7*, 201–211. [CrossRef]
64. Lawson, N.C.; Janyavula, S.; Syklawer, S.; McLaren, E.A.; Burgess, J.O. Wear of enamel opposing zirconia and lithium disilicate after adjustment, polishing and glazing. *J. Dent.* **2014**, *42*, 1586–1591. [CrossRef]
65. Jones, C.; Billington, R.; Pearson, G. The in vivo perception of roughness of restorations. *Br. Dent. J.* **2004**, *196*, 42–45. [CrossRef]
66. ASM. *Friction, Lubrication, and Wear Technology*; ASM International: Materials Park, OH, USA, 1994.
67. Whitehead, S.A.; Shearer, A.C.; Watts, D.C.; Wilson, N.H. Comparison of methods for measuring surface roughness of ceramic. *J. Oral Rehabil.* **1995**, *22*, 421–427. [CrossRef]
68. Tholt de Vasconcellos, B.; Miranda-Júnior, W.G.; Prioli, R.; Thompson, J.; Oda, M. Surface roughness in ceramics with different finishing techniques using atomic force microscope and profilometer. *Oper. Dent.* **2006**, *31*, 442–449. [CrossRef] [PubMed]
69. Baysan, A.; Sleibi, A.; Ozel, B.; Anderson, P. The quantification of surface roughness on root caries using Noncontact Optical Profilometry—An in vitro study. *Lasers. Dent. Sci.* **2018**, *2*, 229–237. [CrossRef]
70. Theocharopoulos, A.; Zou, L.; Hill, R.; Cattell, M. Wear quantification of human enamel and dental glass–ceramics using white light profilometry. *Wear* **2010**, *269*, 930–936. [CrossRef]
71. Litwin, D.; Galas, J.; Blocki, N. Variable Wavelength Profilometry. In Proceedings of the Symposium on Photonics Technologies, Wroclaw, Poland, 12–14 October 2006; pp. 476–479.
72. Moldoveanu, S.C.; David, V. *Selection of the HPLC Method in Chemical Analysis*; Elsevier: Boston, MA, USA, 2017.
73. Law, K.Y. Definitions for Hydrophilicity, Hydrophobicity, and Superhydrophobicity: Getting the Basics Right. *J. Phys. Chem. Lett.* **2014**, *5*, 686–688. [CrossRef]
74. Liber-Kneć, A.; Łagan, S. Surface testing of dental biomaterials—Determination of contact angle and surface free energy. *Materials* **2021**, *14*, 2716. [CrossRef]
75. Alghunaim, A.; Kirdponpattara, S.; Newby, B.-m.Z. Techniques for determining contact angle and wettability of powders. *Powder Technol.* **2016**, *287*, 201–215. [CrossRef]
76. Eibach, T.F.; Fell, D.; Nguyen, H.; Butt, H.-J.; Auernhammer, G.K. Measuring contact angle and meniscus shape with a reflected laser beam. *Rev. Sci. Instrum.* **2014**, *85*, 013703. [CrossRef]
77. Wenzel, R.N. Resistance of solid surfaces to wetting by water. *Ind. Eng. Chem.* **1936**, *28*, 988–994. [CrossRef]

78. Tu, Y.; Ren, H.; He, Y.; Ying, J.; Chen, Y. Interaction between microorganisms and dental material surfaces: General concepts and research progress. *J. Oral Microbiol.* **2023**, *15*, 2196897. [CrossRef]
79. Ho, G.W.; Matinlinna, J.P. Insights on ceramics as dental materials. Part II: Chemical surface treatments. *Silicon* **2011**, *3*, 117–123. [CrossRef]
80. Kreve, S.; Dos Reis, A.C. Effect of surface properties of ceramic materials on bacterial adhesion: A systematic review. *J. Esthet. Restor. Dent.* **2022**, *34*, 461–472. [CrossRef] [PubMed]
81. Paravina, R.D.; Powers, J.M. *Esthetic Color Training in Dentistry*; Mosby: Maryland Heights, MI, USA; Elsevier Mosby: St. Louis, MO, USA, 2004.
82. Bona, D. *Color and Appearance in Dentistry*; Springer International Publishing: London, UK, 2020.
83. Chang, J.-Y.; Chen, W.-C.; Huang, T.-K.; Wang, J.-C.; Fu, P.-S.; Chen, J.-H.; Hung, C.-C. Evaluating the accuracy of tooth color measurement by combining the Munsell color system and dental colorimeter. *Kaohsiung J. Med. Sci.* **2012**, *28*, 490–494. [CrossRef] [PubMed]
84. del Mar Pérez, M.; Ghinea, R.; Rivas, M.J.; Yebra, A.; Ionescu, A.M.; Paravina, R.D.; Herrera, L.J. Development of a customized whiteness index for dentistry based on CIELAB color space. *Dent. Mater.* **2016**, *32*, 461–467. [CrossRef] [PubMed]
85. Della Bona, A.; Pecho, O.E.; Ghinea, R.; Cardona, J.C.; Pérez, M.M. Colour parameters and shade correspondence of CAD–CAM ceramic systems. *J. Dent.* **2015**, *43*, 726–734. [CrossRef]
86. Sharma, G.; Wu, W.; Dalal, E.N. The CIEDE2000 color-difference formula: Implementation notes, supplementary test data, and mathematical observations. *Color Res. Appl.* **2005**, *30*, 21–30. [CrossRef]
87. Paravina, R.D.; Pérez, M.M.; Ghinea, R. Acceptability and perceptibility thresholds in dentistry: A comprehensive review of clinical and research applications. *J. Esthet. Restor. Dent.* **2019**, *31*, 103–112. [CrossRef]
88. Chu, S.J.; Trushkowsky, R.D.; Paravina, R.D. Dental color matching instruments and systems. Review of clinical and research aspects. *J. Dent.* **2010**, *38* (Suppl. 2), e2–e16. [CrossRef]
89. Li, Q.; Yu, H.; Wang, Y.N. Spectrophotometric evaluation of the optical influence of core build-up composites on all-ceramic materials. *Dent. Mater.* **2009**, *25*, 158–165. [CrossRef]
90. Chen, Y.M.; Smales, R.J.; Yip, K.H.; Sung, W.J. Translucency and biaxial flexural strength of four ceramic core materials. *Dent. Mater.* **2008**, *24*, 1506–1511. [CrossRef]
91. Bayindir, F.; Kuo, S.; Johnston, W.M.; Wee, A.G. Coverage error of three conceptually different shade guide systems to vital unrestored dentition. *J. Prosthet. Dent.* **2007**, *98*, 175–185. [CrossRef]
92. Lim, H.N.; Yu, B.; Lee, Y.K. Spectroradiometric and spectrophotometric translucency of ceramic materials. *J. Prosthet. Dent.* **2010**, *104*, 239–246. [CrossRef]
93. Hosoya, Y.; Shiraishi, T.; Odatsu, T.; Ogata, T.; Miyazaki, M.; Powers, J.M. Effects of specular component and polishing on color of resin composites. *J. Oral Sci.* **2010**, *52*, 599–607. [CrossRef] [PubMed]
94. Kim-Pusateri, S.; Brewer, J.D.; Davis, E.L.; Wee, A.G. Reliability and accuracy of four dental shade-matching devices. *J. Prosthet. Dent.* **2009**, *101*, 193–199. [CrossRef]
95. Karaagaclioglu, L.; Terzioglu, H.; Yilmaz, B.; Yurdukoru, B. In vivo and in vitro assessment of an intraoral dental colorimeter. *J. Prosthodont.* **2010**, *19*, 279–285. [CrossRef]
96. Awad, D.; Stawarczyk, B.; Liebermann, A.; Ilie, N. Translucency of esthetic dental restorative CAD/CAM materials and composite resins with respect to thickness and surface roughness. *J. Prosthet. Dent.* **2015**, *113*, 534–540. [CrossRef] [PubMed]
97. Schabbach, L.M.; dos Santos, B.C.; De Bortoli, L.S.; Fredel, M.C.; Henriques, B. Application of Kubelka-Munk model on the optical characterization of translucent dental zirconia. *Mater. Chem. Phys.* **2021**, *258*, 123994. [CrossRef]
98. Della Bona, A.; Nogueira, A.D.; Pecho, O.E. Optical properties of CAD–CAM ceramic systems. *J. Dent.* **2014**, *42*, 1202–1209. [CrossRef]
99. Barizon, K.T.; Bergeron, C.; Vargas, M.A.; Qian, F.; Cobb, D.S.; Gratton, D.G.; Geraldeli, S. Ceramic materials for porcelain veneers. Part I: Correlation between translucency parameters and contrast ratio. *J. Prosthet. Dent.* **2013**, *110*, 397–401. [CrossRef]
100. Johnston, W.M.; Ma, T.; Kienle, B.H. Translucency parameter of colorants for maxillofacial prostheses. *Int. J. Prosthodont.* **1995**, *8*, 79–86.
101. Lee, Y.K. Translucency of Dental Ceramic, Post and Bracket. *Materials* **2015**, *8*, 7241–7249. [CrossRef]
102. Salas, M.; Lucena, C.; Herrera, L.J.; Yebra, A.; Della Bona, A.; Pérez, M.M. Translucency thresholds for dental materials. *Dent. Mater.* **2018**, *34*, 1168–1174. [CrossRef]
103. Zhang, Y. Making yttria-stabilized tetragonal zirconia translucent. *Dent. Mater.* **2014**, *30*, 1195–1203. [CrossRef]
104. Brodbelt, R.; O'brien, W.; Fan, P. Translucency of dental porcelains. *J. Dent. Res.* **1980**, *59*, 70–75. [CrossRef]
105. Kim, H.-K. Optical and mechanical properties of highly translucent dental zirconia. *Materials* **2020**, *13*, 3395. [CrossRef] [PubMed]
106. Pérez Gómez, M.d.M.; Ghinea, R.I.; Ionescu, A.M.A.; Pecho Yataco, O.E.; Della Bona, A. *Color Science and Its Application in Dentistry*; Springer International Publishing: São Paulo, Brazil, 2020.
107. Ilie, N.; Furtos, G. A Comparative Study of Light Transmission by Various Dental Restorative Materials and the Tooth Structure. *Oper. Dent.* **2020**, *45*, 442–452. [CrossRef]
108. Öztürk, E.; Chiang, Y.-C.; Coşgun, E.; Bolay, Ş.; Hickel, R.; Ilie, N. Effect of resin shades on opacity of ceramic veneers and polymerization efficiency through ceramics. *J. Dent.* **2013**, *41*, e8–e14. [CrossRef] [PubMed]

109. Volpato, C.A.M.; Pereira, M.R.C.; Silva, F.S. Fluorescence of natural teeth and restorative materials, methods for analysis and quantification: A literature review. *J. Esthet. Restor. Dent.* **2018**, *30*, 397–407. [CrossRef] [PubMed]
110. Egen, M.; Braun, L.; Zentel, R.; Tännert, K.; Frese, P.; Reis, O.; Wulf, M. Artificial opals as effect pigments in clear-coatings. *Macromol. Mater. Eng.* **2004**, *289*, 158–163. [CrossRef]
111. Cho, M.-S.; Yu, B.; Lee, Y.-K. Opalescence of all-ceramic core and veneer materials. *Dent. Mater.* **2009**, *25*, 695–702. [CrossRef]
112. Lee, Y.-K. Opalescence of human teeth and dental esthetic restorative materials. *Dent. Mater. J.* **2016**, *35*, 845–854. [CrossRef]
113. Pérez, M.M.; Herrera, L.J.; Carrillo, F.; Pecho, O.E.; Dudea, D.; Gasparik, C.; Ghinea, R.; Della Bona, A. Whiteness difference thresholds in dentistry. *Dent. Mater.* **2019**, *35*, 292–297. [CrossRef] [PubMed]
114. Vichi, A.; Louca, C.; Corciolani, G.; Ferrari, M. Color related to ceramic and zirconia restorations: A review. *Dent. Mater.* **2011**, *27*, 97–108. [CrossRef] [PubMed]
115. The Academy of Prosthodontics; The Academy of Prosthodontics Foundation. *The Glossary of Prosthodontic Terms*, 9th ed.; Elsevier: St. Louis, MO, USA, 2017.
116. Carrabba, M.; Vichi, A.; Vultaggio, G.; Pallari, S.; Paravina, R.; Ferrari, M. Effect of finishing and polishing on the surface roughness and gloss of feldspathic ceramic for chairside CAD/CAM systems. *Oper. Dent.* **2017**, *42*, 175–184. [CrossRef]
117. Fernández-Oliveras, A.; Costa, M.F.; Yebra, A.; Rubiño, M.; Pérez, M.M. Gloss measurements and rugometric inspection in dental biomaterials. *Proc. SPIE. Int. Soc. Opt. Eng.* **2013**, *8785*, 1474–1483.
118. *EN ISO 2813:2014*; Paints and Varnishes-Determination of Gloss Value at 20 Degrees, 60 Degrees and 85 Degrees. International Organization for Standardization: Geneva, Switzerland, 2014.
119. da Costa, J.B.; Ferracane, J.L.; Amaya-Pajares, S.; Pfefferkorn, F. Visually acceptable gloss threshold for resin composite and polishing systems. *J. Am. Dent. Assoc.* **2021**, *152*, 385–392. [CrossRef] [PubMed]
120. Rocha, R.; Fagundes, T.; Caneppele, T.; Bresciani, E. Perceptibility and Acceptability of Surface Gloss Variations in Dentistry. *Oper. Dent.* **2020**, *45*, 134–142. [CrossRef]
121. Leonard, D.L.; Charlton, D.G.; Roberts, H.W.; Cohen, M.E. Polymerization efficiency of LED curing lights. *J. Esthet. Restor. Dent.* **2002**, *14*, 286–295. [CrossRef]
122. Price, R.B.; Ferracane, J.L.; Hickel, R.; Sullivan, B. The light-curing unit: An essential piece of dental equipment. *Int. Dent. J.* **2020**, *70*, 407–417. [CrossRef]
123. *BS EN ISO 10650:2018*; Dentistry-Powered Polymerization Activators. International Organization for Standardization: Geneva, Switzerland, 2018.
124. Pacheco, R.R.; Carvalho, A.O.; André, C.B.; Ayres, A.P.A.; de Sá, R.B.C.; Dias, T.M.; Rueggeberg, F.A.; Giannini, M. Effect of indirect restorative material and thickness on light transmission at different wavelengths. *J. Prosthodont. Res.* **2019**, *63*, 232–238. [CrossRef]
125. Price, R.B.; Felix, C.A.; Andreou, P. Effects of resin composite composition and irradiation distance on the performance of curing lights. *Biomaterials* **2004**, *25*, 4465–4477. [CrossRef]
126. Vinagre, A.; Ramos, J.C.; Rebelo, C.; Basto, J.F.; Messias, A.; Alberto, N.; Nogueira, R. Pulp Temperature Rise Induced by Light-Emitting Diode Light-Curing Units Using an Ex Vivo Model. *Materials.* **2019**, *12*, 411. [CrossRef]
127. Price, R.B.; Ferracane, J.L.; Shortall, A.C. Light-Curing Units: A Review of What We Need to Know. *J. Dent. Res.* **2015**, *94*, 1179–1186. [CrossRef]
128. Beolchi, R.S.; Moura-Netto, C.; Palo, R.M.; Rocha Gomes Torres, C.; Pelissier, B. Changes in irradiance and energy density in relation to different curing distances. *Braz. Oral Res.* **2015**, *29*. [CrossRef] [PubMed]
129. Algamaiah, H.; Silikas, N.; Watts, D.C. Polymerization shrinkage and shrinkage stress development in ultra-rapid photo-polymerized bulk fill resin composites. *Dent. Mater.* **2021**, *37*, 559–567. [CrossRef]
130. Lee, Y.-K.; Lim, B.-S.; Kim, C.-W. Influence of illuminating and viewing aperture size on the color of dental resin composites. *Dent. Mater.* **2004**, *20*, 116–123. [CrossRef] [PubMed]
131. Alghazzawi, T.F.; Janowski, G.M.; Ning, H.; Eberhardt, A.W. Qualitative SEM analysis of fracture surfaces for dental ceramics and polymers broken by flexural strength testing and crown compression. *J. Prosthodont.* **2023**, *32*, 100–110. [CrossRef]
132. Inkson, B.J. *Materials Characterization Using Nondestructive Evaluation (NDE) Methods*; Woodhead Publishing: Cambridge, UK, 2016.
133. Bunaciu, A.A.; UdriŞTioiu, E.G.; Aboul-Enein, H.Y. X-ray diffraction: Instrumentation and applications. *Crit. Rev. Anal. Chem.* **2015**, *45*, 289–299. [CrossRef] [PubMed]
134. Patterson, A.L. The Scherrer Formula for X-Ray Particle Size Determination. *Phys. Rev.* **1939**, *56*, 978–982. [CrossRef]
135. Jansen, D.; Goetz-Neunhoeffer, F.; Lothenbach, B.; Neubauer, J. The early hydration of Ordinary Portland Cement (OPC): An approach comparing measured heat flow with calculated heat flow from QXRD. *Cem. Conc. Res.* **2012**, *42*, 134–138. [CrossRef]
136. Prince, E. *International Tables for Crystallography, Volume C: Mathematical, Physical and Chemical Tables*; Springer: Berlin/Heidelberg, Germany, 2004.
137. Uo, M.; Wada, T.; Sugiyama, T. Applications of X-ray fluorescence analysis (XRF) to dental and medical specimens. *Jpn Dent. Sci. Rev.* **2015**, *51*, 2–9. [CrossRef]
138. Kaczmarek, K.; Leniart, A.; Lapinska, B.; Skrzypek, S.; Lukomska-Szymanska, M. Selected Spectroscopic Techniques for Surface Analysis of Dental Materials: A Narrative Review. *Materials* **2021**, *14*, 2624. [CrossRef] [PubMed]
139. Sacher, E.; França, R. Surface Analysis Techniques for Dental Materials. *Dent. Biomater.* **2018**, *2*, 1–31.

140. Fuss, T.; Moguš-Milanković, A.; Ray, C.S.; Lesher, C.E.; Youngman, R.; Day, D.E. Ex situ XRD, TEM, IR, Raman and NMR spectroscopy of crystallization of lithium disilicate glass at high pressure. *J. Non-Cryst. Solids* **2006**, *352*, 4101–4111. [CrossRef]
141. Tzanakakis, E.; Kontonasaki, E.; Voyiatzis, G.; Andrikopoulos, K.; Tzoutzas, I. Surface characterization of monolithic zirconia submitted to different surface treatments applying optical interferometry and raman spectrometry. *Dent. Mater. J.* **2020**, *39*, 111–117. [CrossRef] [PubMed]
142. Miranda, J.S.; Barcellos, A.S.d.P.; Campos, T.M.B.; Cesar, P.F.; Amaral, M.; Kimpara, E.T. Effect of repeated firings and staining on the mechanical behavior and composition of lithium disilicate. *Dent. Mater.* **2020**, *36*, e149–e157. [CrossRef]
143. Isgrò, G.; Kleverlaan, C.J.; Wang, H.; Feilzer, A.J. Thermal dimensional behavior of dental ceramics. *Biomaterials* **2004**, *25*, 2447–2453. [CrossRef] [PubMed]
144. Montazerian, M.; Baino, F.; Fiume, E.; Migneco, C.; Alaghmandfard, A.; Sedighi, O.; DeCeanne, A.V.; Wilkinson, C.J.; Mauro, J.C. Glass-ceramics in dentistry: Fundamentals, technologies, experimental techniques, applications, and open issues. *Prog. Mater. Sci.* **2023**, *132*, 101023. [CrossRef]
145. Theodorou, G.S.; Patsiaoura, D.; Kontonasaki, E.; Chrissafis, K. Thermal Analysis of Glass-Ceramics and Composites in Biomedical and Dental Sciences. In *Thermodynamics and Biophysics of Biomedical Nanosystems*; Springer: Singapore, 2019.